Appendix C.

Geochemical Considerations Regarding the Gold King Mine Release

Contents

List of Tables 3
List of Figures 4
Abstract 5
Background 6
Summary of sampling and analyses used in this report 9
Characterization of the release volume and chemistry 9
Assessment of the fate of solutes in the release waters as they enter the Animas River 11
Analytical considerations 19
Referenc 20

Intent: This geochemical assessment is part of a larger series of EPA/ORD assessments. Raw data, upon which this geochemical assessment is based, are not tabulated herein. Physical transport and related assessments also are not addressed here.

List of Tables

Table C-1. Samples useful for characterizing release-water composition. 32

Table C-2. Conservative estimate of composition of release waters that flowed from Cement Creek into the Animas River. 34

Table C-3. Abiotic Fe^{2+} oxidation half-life at P_{O2} = 0.2 atm. calculated as a function of pH, using kinetic data of Singer and Stumm 35

Table C-4. Properties assumed in thermodynamic reaction-progress modeling of plume waters flowing into the Animas River 37

Table C-5. Typical particle size, diagenetic times for selected Al and Fe oxides under surficial conditions 44

Table C-6. Estimation of dissolved metal concentrations in equilibrium with $Fe(OH)_3$ solids at the pH of the Animas River and Comparison with Observed Values at Four River Locations 45

List of Figures

Figure C-1. Location of Gold King Mine, north of Silverton, in the Cement Creek watershed..... 26

Figure C-2. Geologic map of the area surrounding Gold King Mine.)..... 27

Figure C-3. Map depicting footprints for Gold King Mine. 28

Figure C-4. Aerial trace and profile of a cross-section through Sunnyside and Gold King mines..... 29

Figure C-5. Potential energy (for which low energy is relatively stable) vs reaction progress.. 30

Figure C-6. Hydrograph at gage CC48 on Cement Creek, for August 5, 2015. 31

Figure C-7. Cation/anion balance for water samples from CC06, GKM13, and CC14th Street Bridge. 33

Figure C-8. Saturation Indices (SIs) for calcite (A) and dolomite (B) vs distance from Gold King Mine. 36

Figure C-9. Simulation of the reaction of "Peak Concentration" release waters (Table 2) flowing from Cement Creek with Animas River alkalinity. 38

Figure C-10. Simulation of reaction of Plume + Background Mean concentrations with Animas alkalinity. 39

Figure C-11. Masses of minerals precipitated from the release waters (and Cement Creek water flowing with release waters) as these waters intermingled and reacted with Animas River water as estimated from thermodynamic modeling of titration of "Plume + Background Mean" water with calcite alkalinity that is present in the Animas (Figure 10).. 40

Figure C-12. Simulation of the reaction of Cement Creek Background Mean solutes with Animas alkalinity. 41

Figure C-13. Saturation indices (SIs) with respect to gibbsite ($Al(OH)_3$) vs distance from Gold King Mine. 42

Figure C-14. Saturation indices (SIs) with respect to ferrihydrite ($Fe(OH)_3$) vs distance from Gold King Mine. 43

Figure C-15. Stability fields of ferric oxide minerals as a function of [Fe^{3+}] and pH, with [$SO_4^{=}$] = 90 mg/l, similar to conditions expected in the upper Animas. 46

Figure C-16. Stability fields of aluminum oxide minerals as a function of [Al^{3+}] and pH, with [$SO_4^{=}$] = 90 mg/l, similar to conditions expected in the upper Animas. 47

Abstract

On August 5, 2015, starting at ~11 AM, a dammed drift entry to the Gold King Mine, near Silverton, CO, was breached, releasing a minepool of acidic mine drainage (AMD) estimated to be roughly 11.4 million liters. Using sample data, estimated release volume and very conservative assumptions, the dominant solutes in the release waters that migrated to the Animas River were $SO_4^=$ (≤138000 kg), Ca (≤31100 kg), Al (≤6550 kg), and Fe (≤3530 kg). Acidity load was calculated to be ≤54000 kg $CaCO_3$. The higher loadings for trace elements included Zn (1790 kg) and Cu (730 kg), with other trace elements present at lower loadings Co (14 kg), Pb (12 kg), Cd (7.2 kg) and Ni (6.2 kg).

These release waters cascaded downslope to Cement Creek, entraining and suspending large quantities of spoil, soil and sediments. Based on the data available, e.g., apparent increases in Al and Ca, substantial amounts of soluble salt minerals likely were suspended and partially dissolved in the turbulent flow of the waters as they cascaded to Cement Creek or perhaps flooded stream valleys to suspend overbank sediments. Depending on the mineralogy, dissolution of these salts likely would have affected pH as quickly as the salts dissolved.

The Cement Creek watershed is mapped as containing roughly 100 mines, with four mines alone reported to have been discharging 2300 to 3000 liters/minute (L/m) of untreated AMD. Consequently, Cement Creek is severely degraded, having low pHs and high metals content. Given the low pHs typical of Cement Creek, few chemical changes likely occurred in the release waters during the short residence time in Cement Creek, mainly ranging from 2 to 17 hrs.

Both upstream and downstream of Cement Creek, the Animas River is buffered at moderately alkaline pHs by bedrock including carbonate and chlorite minerals. When the acidic release waters flowed from Cement Creek into the Animas, starting at ~1 PM: i) pH in the mixing waters increased quickly, dramatically accelerating the rate of Fe oxidation; ii) major AMD solutes, including Fe, Al, and Mn, quickly precipitated as incipient oxide-minerals, perhaps including transitory mineral phases; iii) freshly precipitated and/or suspended soluble salt mineral phases, that had been near equilibrium with solutes, would have dissolved, and reprecipitated as oxides in the case of Al and Fe; and iv) trace metals would have sorbed and/or entered solid solution with the Al and Fe oxides.

Based on hydrograph data in Cement Creek near the confluence with the Animas, effectively all of the release waters flowed into the Animas over a 17.25 hour period. For flow rates and alkalinities likely present in the Animas at the time of the release, the calculated acidity load could have been neutralized by roughly two days of Animas flow at most, and probably less. Calculations for calcite saturation suggest that the release acidity was effectively neutralized by about ~150 km downstream from Gold King Mine in the Animas River.

Neutralization of the Gold King acidity generated colloidal solids as reaction products including amorphous and short-range-ordered $Fe(OH)_3$, $Al(OH)_3$ and Mn oxyhydroxides, resulting in yellow coloration in the Animas River. These colloids scavenged the dissolved trace metals in the release waters. Data for lower Animas River show that dissolved metal concentrations were low, µg/L levels and less. Calculations of sorption equilibration of these trace metals, including Zn, Cu and Pb, on $Fe(OH)_3$ surfaces yield modeled concentrations that are consistent with observation, supporting that partitioning to the freshly precipitated colloids was a dominant mechanism that decreased dissolved concentrations of these trace elements in the lower Animas River.

When investigating AMD and mine outflows, geochemical assessments can be more specific if pH is measured at the time of sample collection, dissolved Fe^{2+}, Fe^{3+}, Al^{3+}, Mn^{2+} and $SO_4^=$ are measured,

and acidity is determined by titration. Selective extraction of sediments, perhaps including oxalate and/or dithionite extractions, might aid interpretation of solids formed by reactions of AMD in the environment.

Background

The setting: Gold King Mine is located north of Silverton Colorado (Figure 1), in the southern reaches of the Colorado Mineral Belt. The oldest rock in the region includes late Precambrian (>540M years) sedimentary, metamorphic and igneous rocks (Luedke and Burbank 1999). During a series of regional volcanic eruptions that took place during the late Paleogene (28-23M years), magma intruded into a northeasterly striking shear zone, altering preexisting rock, leaving rich metalliferous sulfide ores and associated hydrothermal enrichments (Luedke and Burbank 1999). The ores are mainly vein-type deposits but extensive volumes of rock are pyritized around the vein zones. In present day, mineralized relict calderas remain, including the Silverton caldera (Figure 2), just north and west of the town of Silverton, and in which Gold King Mine is situated (Yager and Bove 2002).

These sulfide deposits largely were composed of iron (e.g., pyrite), copper (chalcopyrite), lead, zinc, mercury and arsenic (Luedke and Burbank 1999). Notably, gold and silver also were present at anomalous concentrations. With these and other elements present at economic scales the region has been subject to extensive mining for more than a century and today the region is riddled with abandoned mines. These abandoned mines have been generating acid and metals for a century, and regional streams have been extensively contaminated.

The Gold King Mine is situated adjacent to Cement Creek (Figure 1). Cement Creek flows into the Upper Animas River roughly 14 km downstream of Gold King Mine (Figure 1). In turn, the Animas River flows into the San Juan River 192 km downstream of Gold King Mine. The chemistry of Cement Creek is severely impacted with low pHs and high metals from several decades of uncontrolled mining discharges and naturally acidic waters (Schemel and Cox 2005). Today, the Cement Creek watershed is mapped as containing roughly 100 independent mines (US-Mining 2016), and considerably greater than 100 when all mine openings and prospects are mapped (Church et al. 2007).

Until EPA started treating flow from the Gold King Mine after the August 2015 incident, four mines alone (Gold King, Sunnyside with its American Tunnel, Red & Bonita, and Mogul; Figure 3) had been reported as releasing 600 to 800 gallons per minute (2300-3000 L/min.) of untreated acidic mine drainage (AMD) into Cement Creek (Olivarius-Mcallister 2013). Much of the recent discharge from these four mines is thought to result from installation of bulkheads in the American Tunnel in 1996 and 1997 which blocked free flow from Sunnyside Mine, raising regional ground water to discharge at other locations by the early 2000s (Gobla and Gemperline 2015). The spatial relationship and potential hydraulic connection of Gold King Mine with the American Tunnel is depicted in Figure 4.

In stark contrast to Cement Creek, the Animas River is buffered by calcareous rock and maintains moderately alkaline pHs over the reach between Cement Creek and the San Juan River. These moderately alkaline, well-buffered pHs help to suppress dissolved-metal concentrations in the Animas and its waters discharging into the San Juan (Schemel and Cox 2005).

Concerns with mine releases: Mine releases and abandoned mine outflows present two general areas of concern: i) acidity and acid generation; and ii) mobilization of trace and toxic metals.

Acid Generation: Mining voids act as drains for overlying and adjacent land, dropping the groundwater table. When the water table drops, sulfide-rich overburden and mining wastes that previously had been submerged in groundwater containing ~10 ppm O_2 or less, are exposed to air containing up to 21% (208,000 ppm) O_2. These sulfide-mineral ores are highly reduced (electron rich) and, when exposed to oxygen, the minerals oxidize (yield electrons) and dissolve according to the following reactions, using pyrite (FeS_2) as an example (Rose and Cravotta 1998):

$$FeS_2(s) + 3.5O_2 + H_2O \rightarrow Fe^{2+} + 2SO_4^{=} + 2H^+ \quad (1)$$

$$Fe^{2+} + 0.25O_2 + H^+ \rightarrow Fe^{3+} + 0.5H_2O \quad (2)$$

$$FeS_2(s) + 14Fe^{3+} + 8H_2O \rightarrow 15Fe^{2+} + 2SO_4^{=} + 16H^+ \quad (3)$$

Reactions 1 and 3 of these oxidation and dissolution reactions generate acidity, i.e., H^+. When the dissolved metallic products of Reactions 1 through 3 are exposed to oxidizing and moderate-pH conditions, either through time or via migration of the metal-bearing waters, the major metals precipitate as authigenic (formed in place) amorphous solids and mineral phases.

When mine discharges occur in low flows, or by diffuse groundwater discharge, often the dominant part of these authigenic solids are stable crystalline oxide minerals (e.g., hematite and goethite for iron minerals), minerals that occur abundantly in pristine soils and sediments as well as areas affected by acidic mine drainage (AMD). In contrast, when large volumes of AMD are introduced suddenly into the environment as with a release, the relatively slow crystallization processes that are required to form stable crystalline minerals do not have time to take place and incipient amorphous to short-range-ordered crystalline phases are the dominant minerals to form (Figure 5). Over days to years, depending on chemical conditions, these incipient solids recrystallize to stable mineral phases (Figure 5). The stoichiometry for these intermediate amorphous and mineral phases can be given as:

$$Fe^{3+} + 3H_2O \rightarrow Fe(OH)_3(s) + 3H^+ \quad (4)$$

$$Mn^{4+} + 2H_2O \rightarrow MnO_2(s) + 4H^+ \quad (5)$$

$$Al^{3+} + 3H_2O \rightarrow Al(OH)_3(s) + 3H^+ \quad (6)$$

The incipient solids formed in Reactions 4-6 are prominent after large releases of AMD, being visible as yellow (and perhaps red, white or black) staining in rivers of moderate pHs. The stains arising from large AMD releases commonly are called "yellowboy".

Each of these precipitation reactions, Reactions 4-6, generate additional acid, augmenting acidity generated by oxidation, Reactions 1 and 3. All these acid-generating reactions can take place after migrating in water over considerable distances from the source, so that pH actually can decrease as the waters flow away from a mine source. Iron and manganese are multivalent, and these metals often are present in their reduced, more soluble divalent state. Numerous minerals can form from higher-valence oxidized iron and manganese species, which can cause precipitation of these metals to proceed dominantly after these cations are oxidized. Manganese oxidation, in particular, can proceed slowly, even more so than iron (Skousen et al. 1998). Also, the mineralogy of the manganese oxide minerals varies as a sensitive function of numerous variables, so the stoichiometry of the acid production for manganese precipitation can be variable.

Importantly, Reactions 4-6 commonly occur during periods of low mine discharge as well as after releases. However, when mine flow is slow and/or diffuse, the rate at which these incipient phases are generated is counterbalanced by recrystallization to form more stable minerals which tend to become entrained in, and/or adhered to, streambed sediments. As a result, under low-flow conditions, these intermediate phases often can be observed only over limited areas. During periods of slow AMD releases, the prominent "yellowboy" commonly is not visible over long reaches of streams; nevertheless, the stable secondary mineral products of AMD oxidation and neutralization are ubiquitously distributed over long reaches of streams downgradient of long-term mine releases. These stable solids commonly are visible in streambeds and soils as red to yellowish brown (Fe), white (Al) and black (Mn) stains.

As a consequence of all the above, the acidity of AMD often is composed dominantly of the free acidity of H^+, as well as Fe, Al and Mn, and AMD acidity is estimated reasonably well by the equation (Rose and Cravotta 1998):

$$Acidity = 50\left\{\frac{3[Fe^{3+}]+2[Fe^{2+}]}{55.85} + \frac{3[Al^{3+}]}{26.98} + \frac{2[Mn^{2+}]}{54.94} + 10^{(3-pH)}\right\} \qquad (7)$$

where acidity has units of mg $CaCO_3$/L, the metals are mg/L and pH is in standard units. If pH exceeds the first hydrolysis constant for Fe^{3+}, pH~2.2, Equation 7 requires modification for hydrolysis. In addition to this calculated value, acidity also can be measured by a titration after addition of H_2O_2 to oxidize Fe and Mn; this procedure is described in EPA Method 305.1. Calculated and measured acidities commonly agree reasonably well but can be discrepant if other metals are present at levels sufficient to add acidity upon precipitation. In order to assess the impact and fate of AMD in the environment with quantitative resolution, it is necessary to calculate or measure the value of acidity.

Trace-metal mobilization: AMD usually is elevated in numerous metals, often including some combination of Zn, Cd, Cu, Pb, As, Hg, Ni, Co, Mo, W, As, Se, Ag and Au among others. When these metals are present at elevated concentrations in, or adjacent to, mineralized zones, they can be mobilized as acid conditions are generated by sulfide dissolution and/or oxide-mineral precipitation.

As AMD waters are neutralized in the environment, the mobility of most of these trace metals decreases dramatically. Under moderate-pH, oxidizing conditions, the dissolved concentrations of

these metals tend to be limited by specific and electrostatic sorption to authigenic Fe, Al and Mn oxide minerals, both the incipient and stable mineral phases (Rose 1979). Secondary sinks under these conditions include electrostatic sorption to aluminosilicate clays and chelation with natural organic matter.

Summary of sampling and analyses used in this report

The Gold King Mine release occurred on August 5, 2015, flowing from the mine breach into nearby Cement Creek. Interpretations in this report regarding the impact and fate of this release are based on samples collected by the EPA and other government entities, and include: i) roughly 500 water-sampling events, ranging from the mine to 550 km downstream, well into the San Juan River, and from the time of the release until 28 days after the release; ii) water samples were analyzed for up to 60 dissolved and total chemical properties; iii) roughly 320 sediment samples, ranging from the 12.5 to 640 km downstream, well into the San Juan River, and from the time of the release until more than 27 days after the release; and iv) sediment samples were extracted by EPA Method 3050B, a hot concentrated-acid extraction that dissolves most metals in the primary and authigenic mineral phases.

Characterization of the release volume and chemistry

The timing and volume of the mine release have been estimated by staff at USEPA/Athens, GA using data from a stream gage on Cement Creek, roughly 12.5 km downstream of the mine and designated herein as location "CC48" (Figure 6). Based on interpretation of these data, excess water from the mine release flowed past CC48 from roughly 12:45 PM until 6:00 AM, a period of 17.25 hours. Based on the data from CC48, the volume of the release was 11,420,000 liters.

Our best estimates of the composition of the mine release centrally are from three sampling events (with some additional data from later samples): i) water samples collected from the mine opening (designated as location CC06) on August 15, ten days after the release; ii) water samples collected from where Gold King discharge flows from a tributary into Cement Creek (GKM13), 0.9 km from the mine opening, ten days after the release on August 15; and iii) water samples collected from the "14th Street Bridge" (designated CC 14th St Bridge), ~13 km down Cement Creek from Gold King Mine, on August 5 at 4 PM (roughly three hours after maximum flow at sample point CC48 one kilometer upstream from the 14th Street Bridge; Figure 6). Both total and dissolved analytes are reported for these samples (Table 1). Total analytes include the dissolved portion plus suspended material, the large majority of which is stable natural mineral grains that are denser than water and can be expected to settle out of the water column as flow velocity decreases. Dissolved analytes are the more mobile fraction and, therefore, the fate of the dissolved fraction generally is of greater concern. The fate of dissolved constituents can be interpreted with standard geochemical approaches. This geochemical report focuses on the dissolved chemical data and generally will not address the suspended fraction except as it relates to the dissolved fraction through precipitation, sorption or dissolution reactions.

The completeness and internal consistence of these samples, both within and between samples, can be assessed with cation-anion charge balances (Figure 7). Trace species having multiple oxidation states represented in Figure 7 were assigned a valence, and charge for oxyanions, based on professional judgement because equilibrium cannot be assumed for polyvalent trace elements. The charge balances for CC06 and GKM13 are 0.986 and 1.043, respectively, indicating good internal consistence between cations and anions, and suggesting that i) all major cations and anions are represented in these analyses and ii) judged trace speciation was qualitatively reasonable.

For the purposes of estimating the composition of the August 5 release, also noteworthy on Figure 7 is that the August 5 sample drawn from the release waters mixed with Cement Creek (CC 14th St Bridge), has a higher total concentration of cations than do the August 15, post-release waters collected near the mine, i.e., CC06 and GKM13. The most prominent differences of CC 14th St Bridge from the other two samples is that Ca and Al are more concentrated and Fe is less concentrated (Figure 7). These observations suggest that i) the original release waters differed from water flowing from Gold King on August 15, and/or ii) that release waters entrained solutes as the waters flowed from the mine and down Cement Creek toward the Animas River. Later in this report, I argue that most of the remediation of the release waters occurred in the Animas River. Within this context, the "release source" is best thought of as what flowed from Cement Creek into the Animas River. As such, the CC 14th St sample offers unique insight to the quality of the actual release waters. Unfortunately, this sample also was diluted substantially by Cement Creek (Figure 6). Mike Cyterski and Kate Sullivan, EPA/Athens, estimated the undiluted quality of the release waters from this sample using:

$$Q_t c_t = Q_r c_r + Q_c c_c \qquad (8)$$

where Q is flow rate (L/min), c is concentration (mg/L), subscript t stands for total (i.e., the composite value of the August 5 sample), subscript r stands for release water (i.e., the value ultimately desired), and subscript c stands for creek (i.e., the value estimated for the Creek in the absence of the mine-water release). Background flow was estimated from USGS gage readings recording before the release waters arrived at the gage and background solute concentrations were estimated from samples collected in Cement Creek days after the release waters had left Cement Creek.

Having solved for the estimated concentrations of the release waters using Equation 8 (solving for c_r), in the interest of generating a conservative estimate of the source, the highest reported value of i) the estimate of c_r using CC14th St data and Equation 8, ii) CC06 data and iii) GKM13 data. Looking at quality of mining-degraded watersheds, Nordstrom (Nordstrom 2011) noted that initial flushes of water leaving watersheds after precipitation events were highly enriched in mining-related solutes. Considering this effect, and in the interest of generating a conservative estimate of the source term, the concentrations were doubled for the first 30 minutes of the release event, to arrive at very conservative upper-limit estimates of the release. These conservative estimates of the source term for the waters released from Cement Creek to the Animas River on August 5, 2015 are summarized in Table 2.

The CC 14th St Bridge sample did not include a measured pH. In the interest of remaining conservative, I assume the pH of CC 14th was the same as that measured in Gold King Mine sample CC06, pH=2.9 (Table 1). The CC 14th sample also did not report a value for $SO_4^=$. Referring to Figure 7, the anions in samples CC06 and GKM13 are comprised almost entirely of $SO_4^=$. Based on this observation, I estimated $SO_4^=$ for CC14th and for the release waters by charge balance with the cations (Table 2). Then I used Equation 7 to estimate acidity of these source waters (Table 2).

These estimates of the release-water composition as it entered Animas River (Table 2) are very conservative and likely to overestimate actual composition. Because of dilution, and neutralization by salts and other minerals, pH likely was higher than the assumed 2.9, and the solubility of numerous minerals is highly sensitive to pH in this range. Even in the unlikely case that pH in the Creek was 2.9, assuming a water temperature of 8 °C in Cement Creek, calculations performed in

Geochemist's Workbench (Bethke 1998) indicate the Peak Concentration estimated in Table 2 is supersaturated with gypsum ($CaSO_4 \cdot 2H_2O$) as well as other minerals. Calculation of this supersaturated condition supports the notion that these estimates of release water composition (Table 2) are, indeed, conservative and likely to overstate the concentrations of at least some solutes.

The fate of iron in surficial settings depends on its valence state which was not determined in these samples. In "The Setting" section of this manuscript, it was argued that much of the discharge waters arose from deep pools of regionally interconnected mines that had been sealed from the atmosphere by bulkheads. This sealed state and the large scales of the mine pools, suggests that O_2 was in short supply. In addition, reaction of Fe^{3+} with pyrite (Reaction 3) proceeds strongly to the right, yielding Fe^{2+} and $SO_4^{=}$, with an equilibrium constant of log K~99 (Bethke 1998). And numerous kinetic studies have shown that, at acidic pHs, oxidation of pyrite by Fe^{3+} (Reaction 3) proceeds much more quickly than it does with O_2 (Reaction 1) (Rose and Cravotta 1998). Based on expected paucity of O_2 in the mine waters and propensity for pyrite oxidation to proceed exhaustively and quickly by Fe^{3+}, the oxidation state of Fe in the source waters at Gold King Mine likely was dominantly ferrous, Fe^{2+}.

The abiotic oxidation of Fe^{2+} under oxidizing, acidic conditions is quite slow (Washington et al. 2004), with a half-life of roughly 7 years at pH 4 and roughly 60 years at pH 3 and less (Table 3; Appendix 1) (Singer and Stumm 1970). Microbes can accelerate Fe^{2+} oxidation rate (Rose and Cravotta 1998), and probably Fe-oxidizing bacteria were entrained in the disaggregated spoil at the Gold King mine opening that was eroded during the breach event (Youtube 2015) and carried as suspended load down Cement Creek. Nevertheless, it seems likely that most of the dissolved Fe in the release waters remained reduced during the hours-long transit down Cement Creek. Consequently, the chemical composition of the release waters likely changed little during the short time it took to flow down Cement Creek, other than perhaps alternately dissolving and precipitating Ca^{2+}, and perhaps other, $SO_4^{=}$ salts as the release waters flowed over normally dry lands above the Creek banks.

Assessment of the fate of solutes in the release waters as they enter the Animas River

In contrast to Cement Creek, the Animas River is buffered by calcareous bedrock above the confluence with Cement Creek (Desborough and Yager 2000, Schemel and Cox 2005). Immediately upstream of Cement Creek, the Animas drains the Silverton Volcanics that are chiefly composed of volcaniclastic sediments, including calcite which often is "pervasive and disseminated throughout the groundmass and within microveinlets," and, "where not intensely altered," "has the ability to buffer acidic waters" (Yager and Bove 2002). The Silverton Volcanics also include chlorite (Yager and Bove 2002), which can enhance alkalinity as well (Desborough and Yager 2000). Buffering capacity likely is enhanced still more about one kilometer downstream of Silverton where the Animas transects numerous pre-Tertiary sedimentary beds including numerous lithologic units of limestone and calcareous shale (Yager and Bove 2002). The alkalinity of these waters is important for its potential to neutralize the acidity of the Gold King release. For example, for acidity generated from Al^{3+} (Reaction 6):

$$CaCO_{3(s)} + Al^{3+} + 3H_2O \rightarrow 3Ca^{2+} + 3HCO_3^{-} + Al(OH)_{3(s)} \quad (9)$$

Given this geologic setting, and using the data collected for this study, saturation indices (SIs) were calculated, using thermodynamic data reported in Parizek et al. (Parizek et al. 1971), for calcite ($CaCO_3$) and dolomite ($CaMg(CO_3)_2$) downstream of the Gold King Mine including Cement Creek, the Animas River and into the San Juan River (Figure 8A & 8B; Appendix 2). Negative SI values indicate that water is undersaturated with a mineral phase, values of near zero indicate the water roughly is in equilibrium with mineral, and positive SI values suggest the mineral should precipitate from solution. SIs are generated from thermodynamic data and need to account for the deviation of the real aqueous solution from an ideal thermodynamic condition using activity coefficients (ϒ). Activity coefficients require knowledge of the ionic strength (I) of the solution. The value of I, is calculated using the concentrations of all major solutes. So calculation of mineral SIs requires a complete suite of major-chemical analytes; however, many of the samples in this study include data only for selected species, major and toxic metals for example. Consequently, to accommodate this dataset, I was calculated for those samples that were subjected to analysis for all major analytes. Speciation of these analytes (e.g., Al^{3+} vs $Al(OH)_2^+$) was estimated based on judgement of conditions including reported pH, inferred [O_2] and similar geochemical parameters. Then for these samples, ϒ was calculated using the Extended Debye-Huckel Equation (Stumm and Morgan 1981). Samples having an incomplete suite of analytes were assigned values of ϒ from geographically nearby samples having similar geochemical characteristics. With all samples/analytes having calculated or estimated values for ϒ, SI values were calculated. Consistent with calculation of I, calculation of ϒ included correction for impact of pH on speciation and assessment for complexation by major solutes (e.g., $SO_4^=$). For these calculations, it was assumed that the river waters equilibrated with atmospheric CO_2, log P_{CO2} = -3.40 (atmospheres units). For samples not having reported values of pH, pH was assigned values of nearby samples having similar reported geochemical analytical profiles. Figures 8A and 8B indicate that the Animas was variably undersaturated with respect to calcite and dolomite immediately downstream of Cement Creek at the time the samples were collected for about 100 km (suggesting the presence of acidity), but that Animas remained roughly saturated with these alkaline minerals for most samples >150 km (suggesting neutralization of acidity in these locations). Additional data for the Animas upstream of its confluence with Cement Creek indicate moderately alkaline conditions as well (data not shown), so the only Animas data indicating pronounced undersaturation with calcite is for samples collected at the confluence with Cement Creek and downstream of this location as far as ~150 km from Gold King mine, collected during the time of the release. Taken altogether, these observations suggest that the acidity of the release water was effectively neutralized at roughly 150 km downstream from the Gold King Mine.

Acidity-Alkalinity Balance of the release waters at the Cement-Animas confluence: Table 2 reports a maximum estimated load of acidity in the mine release as ~54000 kg as $CaCO_3$. Based on interpretation of data from the gage in Cement Creek near the confluence with the Animas, the acidity load flowed into the Animas over a period of roughly 17.25 hours on August 5.

According to data from a gage in the Animas River upstream of Cement Creek, on August 5, flow in the Animas at the confluence with Cement Creek was about 115 ft^3/sec (11.7M liters/hr). Alkalinity has been measured in water samples collected by the EPA from the Animas River upstream of Cement Creek, falling in the range of 30 mg $CaCO_3$/l. As the Animas flows downstream, alkalinity ascends to about 90 mg CaCO3/l, consistent with expectations for waters draining carbonate bedrock. For these values of flow and alkalinity in the Animas, the 54000 kg load of acidity in the release could be neutralized with about 50 to 150 hours of Animas flow without any additional dissolution of carbonate bedrock, roughly three to nine times the time increment of the release from Cement Creek to the Animas. The actual time to neutralize the release waters in the

Animas likely was substantially shorter because, i) the acidity load of the release could well have been much less than the estimates in Table 2 in that these estimates were arrived at with very conservative assumptions, ii) carbonaceous bed sediments or bedrock likely added alkalinity in the acidic release waters as they migrated down the Animas, and iii) downstream tributary inflow might have augmented alkalinity as well.

Accelerated oxidation of Fe in the Animas River: Whereas abiotic oxidation Fe^{2+} half-life is on the order of years to decades at pH≤4, at the moderately alkaline pH values observed in the Animas the oxidation half-life falls to seconds to hours. Using the kinetic data supplied by Singer and Stumm (Singer and Stumm 1970), the ferrous oxidation half-life falls to 7 hr at pH 6, 4 min at pH 7 and 3 sec at pH 8 (Table 3). This generation of Fe^{3+} through oxidation of Fe^{2+} will foster precipitation of amorphous ferric-oxide mineral phases (Reaction 4).

Taken altogether, the combined factors of (i) the saturation indices for calcite suggesting near-saturation for all distances downstream of 150 km (Figure 8), (ii) the capacity of the Animas to neutralize the release load of acidity with <150 hours of flow, and (iii) the accelerated rate of Fe^{2+} oxidation at moderately alkaline pHs (Table 3), constitute compelling evidence that essentially all of the release acidity was neutralized in the Animas River within about 100-150 km of stream distance from Gold King Mine

Precipitation of incipient oxyhydroxide colloidal minerals which dyed the Animas River yellow: The neutralization of mine release waters that took place in the Animas entailed precipitation of Fe^{3+}, Al^{3+} and Mn^{4+} incipient oxide phases of the type shown in Reactions 4-6. The progress of these precipitation reactions has been modeled thermodynamically (Table 4) using Geochemist's Workbench® (Bethke 1998) and the results are depicted in Figures 9-12. Geochemist's Workbench® is well-known commercial software that enables the qualified user to model thermodynamic equilibrium of water, having user-specified properties, with mineral phases, also specified by the user. This modeling can be done toward different objectives, e.g., calculation of equilibrium constants, modeling of reaction progress, and generation of a variety of equilibrium diagrams. In Figures 9-12, Cement Creek waters were reacted with sufficient calcite masses to just saturate the system, mimicking the alkaline state of the Animas as reflected in Figure 8. The reactions were modeled at 11 °C, in equilibrium with 0.208 atmospheres of O_2 and $10^{-3.4}$ atmospheres of CO_2. Silica was modeled as being in approximate equilibrium with quartz. Minerals that were excluded from precipitating in this modeling included: i) primary minerals that typically do not form authigenically in sediments and soils, ii) secondary minerals that commonly form by recrystallization from incipient mineral phases, and iii) crystalline minerals composed of low-level trace elements that more likely were entrained as impurities in dominant mineral phases.

Figure 9 depicts "Peak Flow" (Table 2) concentrations entering the Animas. This figure should include the most complex suite of minerals that might have precipitated during the event. Figure 10 depicts the "Plume + Background Mean" (Table 2) concentrations entering the Animas; these values are the mean estimated concentrations of solutes emitted from Cement Creek during the plume, representing complete mixing of the entire volume of plume and creek waters during the release period. Comparison of Figures 9 and 10 suggests that no unique minerals precipitated solely during release of the most concentrated water. Using the mineral masses depicted in Figure 10, Figure 11 provides estimates of minerals modeled as precipitating from the plume waters in the Animas River. Figure 12 depicts "Creek Background" (Table 2) water reacting with Animas alkalinity. Comparison of Figures 10 and 12 suggests that most mineral species that potentially precipitated during the plume also potentially precipitate from Cement Creek waters as they enter the Animas under normal-flow conditions at other times as well. The only minerals that modeling suggests might have precipitated during plume release but not during the depicted "background" flow (Figure 12) include gypsum ($CaSO_4{\cdot}2H_2O$), alunite ($KAl_3(SO_4)_2(OH)_6$), smithsonite ($ZnCO_3$), and tenorite (CuO).

Alunite is an endmember mineral in the isostructural alunite-jarosite ($KFe_3(SO_4)_2(OH)_6$) family, having a complex set of solid solutions in the cation sites (K^+, Na^+, H_3O^+) (Brophy and Sheridan 1965), and (Al^{3+}, Fe^{3+}, Cu^{2+}, and Zn^{2+}) (Scott 1987), so any alunite-jarosite minerals associated with the plume waters, probably were solid solutions, albeit near end-member. And the isostructural jarosite potentially can precipitate during background-type flows (Figure 12). Whether alunite-jarosite minerals, or other Al and Fe^{3+} hydroxysulfate minerals, actually precipitated in the Animas during this event is uncertain and dealt with in more detail in the next section. Whether smithsonite and tenorite actually precipitated is uncertain as well; considering the trace-level concentrations of Zn^{2+} and Cu^{2+} in the presence of more dominant precipitating mineral phases, most of these metals could have been entrained as impurities in other minerals.

A number of minerals depicted in Figures 9-12 likely are transitory and unstable in the Animas River. This is evident for the alunite-jarosite group in that the masses of these minerals dissolve at 60% to 90% of reaction completion. This is because, as acidity is neutralized by limestone alkalinity, Al^{3+} and Fe^{3+} activity are regulated to progressively lower levels by precipitation of amorphous $Al(OH)_3$ and $Fe(OH)_3$; as Al^{3+} and Fe^{3+} activity drops the ion-activity products (IAPs) for the alunite-jarosite minerals fall below saturation. Effectively, alunite and jarosite (or any hydroxysulfate salts) are replaced by the relatively more stable $Al(OH)_3$ and $Fe(OH)_3$. Figures 9 and 10 depict gypsum ($CaSO_4{\cdot}2H_2O$), dolomite ($CaMg(CO_3)_2$), barite, smithsonite and tenorite as being stable (because they remain at reactions' completion). However, as the plume migrated down the Animas, $SO_4^=$ activity likely dissipated with a resulting dissolution of gypsum, leaving Ca^{2+} activity to be controlled by its normal constraint in the lower Animas, calcite (Figure 8). Likewise, dolomite might well have dissolved if it became undersaturated in the lower Animas (Figure 8). If smithsonite and/or tenorite precipitated, these minerals might well have redissolved as well because Zn and Cu likely are controlled to relatively lower activities by sorption on ferric and aluminum hydroxides as described two sections below.

It is noteworthy, that the Gold King discharge event is not unique in acting as a potential source of Al and Fe^{3+} hydroxysulfate minerals to the Animas River from Cement Creek. In fact, modeling of reaction progress for Cement Creek background waters with Animas alkalinity suggests precipitation of transitory jarosite phases (Figure 12).

Based on the "Plume + Background" data (Figure 10), gypsum comprised the largest load among the unstable minerals in the plume. For the calculated discharge from Cement Creek during plume release of 11.42 ML, roughly 9300 kg of gypsum was carried by, or precipitated from, the plume waters as they mixed with the Animas (Figure 11). Lesser amounts of other unstable minerals (e.g., Al and Fe^{3+} hydroxysulfates) might have precipitated as well. These minerals would have entrained trace metals as impurities in addition to the major solutes, Zn and Cu described above. When these minerals redissolved, the impurities would have entered solution too. The concentrations of these trace impurities then would be subject to the same long-term fate as Zn and Cu, scavenging by stable hydroxide minerals as described two sections below.

Of the remaining minerals depicted in Figures 9-12, gibbsite ($Al(OH)_3$), ferrihydrite ($Fe(OH)_3$) and birnessite (MnO_2) should remain as solids in the Animas, their stability supported by the alkaline pHs of the carbonate-buffered waters. Over time, these solids likely will recrystallize to still-more stable forms such as long-range ordered gibbsite, goethite (FeOOH) and/or hematite (Fe_2O_3). Using the modeling depicted in Figure 10, and the calculated 11.42 ML discharge volume, roughly 3700 kg of gibbsite and 1300 kg of ferrihydrite precipitated in the Animas during the Gold King discharge event (Figure 11). Based on thermodynamic principles, and not kinetic, Figures 9-12 depict birnessite as precipitating before ferrihydrite. Manganese oxidation/precipitation kinetics are slow, however, and Mn likely precipitated only well after ferrihydrite precipitation had initiated (Skousen et al. 1998). Also, Mn mineralogy is complex, the actual precipitating mineral species being

sensitive to a number of variables. Birnessite is common among these mineral species and a suitable representative of Mn chemistry, but the actual mineralogy might differ. Using birnessite as a proxy for authigenic Mn minerals, roughly 800 kg of Mn minerals precipitated in the Animas during the discharge event.

Downstream chemistry data can be used to evaluate the modeling predictions for the stable minerals described above and in Figures 9-12. Using thermodynamic data reported in Geochemist's Workbench (Bethke 1998), for samples having detectable Al^{3+} the SIs for gibbsite ($Al(OH)_3$) are plotted as a function of distance from Gold King Mine in Figure 13. The small positive SI values shown for gibbsite in Figure 13 indicate the waters are saturated with respect to gibbsite and strongly support that gibbsite colloids were suspended in these water samples, just as predicted by the modeling shown in Figures 9-12. This equilibrium of Al with $Al(OH)_3$ in circumneutral waters also has been reported for mine waters by Nordstrom (Nordstrom 2011) and many others.

Using thermodynamic data from Geochemist's Workbench (Bethke 1998) and assuming the oxidation state of dissolved Fe to be ferric as justified by kinetic principles (Table 3), the SIs for ferrihydrite are plotted in Figure 14 for those Animas samples having detectable levels of dissolved Fe. Figure 14 indicates saturation with respect to ferrihydrite, also consistent with the modeling depicted in Figures 9-12.

It is noteworthy that the near-equilibrium calculated for $Al(OH)_3$ and $Fe(OH)_3$ in the lower Animas (Figures 13 and 14) strongly suggests that, even if Al and/or Fe^{3+} transitory hydroxysulfate minerals were transported to, or formed in, the Cement-Animas confluence, either: i) these hydroxysulfate minerals dissolved and were fully replaced by the more stable hydroxides; of ii) dissolution of these hydroxysulfate phases is slow relative to the precipitation of the relatively stable hydroxide phases. In either case, these hydroxide minerals evidently were effective constraints on solution chemistry in the post-event water samples drawn from the lower Animas.

Mineralogy of Al and Fe^{3+} hydroxysulfates as related to plume discharge into the Animas: As noted above, modelling based solely on thermodynamics suggests that alunite-jarosite type minerals might have precipitated during plume release (Figures 9 & 10), and even during normal "background" discharge of Cement Creek (Figure 12). In fact, it seems doubtful that alunite or jarosite precipitated in the Animas at the confluence with Cement Creek, either during plume discharge or at other times.

Addressing alunite and Al hydroxysulfate minerals, according to Bigham and Nordstrom, "for pH values much less than 5.0, dissolved Al behaves as a conservative constituent" (Bigham and Nordstrom 2000). Measurements of pH taken in Cement Creek at Silverton on August 12 and 14, 2015, seven and nine days after the release, were pH = 3.63 and 3.60, so Al hydroxysulfate precipitation was unlikely in Cement Creek. When pH is increased to >5.0, precipitation kinetics seem to favor formation of hydrobasaluminite ($Al_4(SO_4)(OH)_{10}\cdot 10H_2O$) and basaluminite ($Al_4(SO_4)(OH)_{10}\cdot 4H_2O$) because these minerals are found more commonly in low temperature mixing zones while alunite is dominantly observed in acidic hypersaline lakes and zones of hydrothermal alteration (Bigham and Nordstrom 2000). The aluminite minerals are metastable with respect to alunite and gibbsite (Bigham and Nordstrom 2000). Based on the presence of gibbsite and absence of alunite at reactions' completion in Figures 9-12, any aluminite minerals that might have precipitated during admixing of plume and Animas waters would be expected to recrystallize to gibbsite. Bolstering this inference, Figures 9-12 depict modeling of closed geochemical systems, wherein $SO_4^{=}$ is not lost to surroundings; considering that $SO_4^{=}$ was diluted in the open system of the Animas River, gibbsite would be expected to be even more stable relative to alunite than depicted in

these figures. All of this reasoning is strongly supported by the observation that the lower Animas was near equilibrium with gibbsite during the few sampling events when Al was at detectable levels (Figure 13).

Addressing jarosite and Fe^{3+} hydroxysulfate minerals, remembering the arguments presented earlier, that Fe dominantly was in reduced form in Gold King mine water, and Fe oxidation in Cement Creek probably was slow relative to its residence time in Cement Creek, it is unlikely that ferric hydroxysulfate minerals would have formed to any considerable extent in Cement Creek.

However, even if there was some ferric Fe, i) infrequent detection of jarosite in all but the most acidic settings, ii) common observation of supersaturation with jarosite in less acidic settings, and iii) the typically well-ordered lattice of jarosite, all suggest that kinetic barriers might impede jarosite under all but the most acidic environmental conditions (Bigham and Nordstrom 2000). In contrast, schwertmannite ($Fe_8O_8(OH)_6SO_4$) commonly is observed in waters having $2<pH<4$ (Bigham and Nordstrom 2000). Based on experimental and observational evidence Bigham and coworkers have proposed that jarosite tends to form in the range $1.5<pH<2.5$, schwertmannite in the range $2.5<pH<5.5$, and ferrihydrite is favored at $pH>5.5$ (Bigham et al. 1996, Bigham et al. 1996). So if some Fe was present in ferric oxidation state in Gold King Mine, considering that Cement Creek pHs (3.60-3.63 at Silverton) fall in the range for the formation of schwertmannite over jarosite, schwertmannite would be more likely to form in Cement Creek than jarosite. When the plume waters mixed with the more voluminous alkaline waters of the Animas, pH likely ascended to >5.5 and under these conditions, ferrihydrite would be favored over jarosite. Schwertmannite is metastable and, even if it did form in the Animas, it likely recrystallized to ferrihydrite or a stable oxide phase like goethite or hematite.

One possibility that cannot be dismissed is that alunite-jarosite type minerals were present in the spoil or stream banks that were eroded by the plume. If these minerals were suspended in the plume surge, it remains possible that these minerals could have been carried in suspension to the Animas River. It is noteworthy, however, that there are large documented occurrences of jarosite in the Animas watershed. One such occurrence is mapped in the Mineral Creek watershed, whose confluence with the Animas is downstream of Cement Creek. Here, Yager et al. (Yager et al. 2000) mapped a major alteration zone on the flanks of Mount Moly in the Mineral Creek watershed as "quartz-sericite-pyrite (Q-S-P) altered host rock, with jarosite- and goethite-stained surfaces."

Trace element sorption in the incipient mineral phases and long-term occlusion in crystalline oxides: Unlike alumino-silicate clays, which have substantial permanent surface charges, oxide solids dominantly have surface charges that vary with pH and ionic strength (I); at low pH values charge is positive, at high pH values charge is negative, and there is a pH (unique to each oxide solid) at which the surface has a "zero point of charge" (ZPC). The ZPC for ferrihydrite is about 7.9-8.2 (Dzombak and Morel 1990), for goethite it is about 9.0-9.7 (Sverjensky 1994), for hematite about 8.5 (Sverjensky 1994), and for gibbsite about 8.0-9.2 (Hsu 1989) (Table 5). As a consequence of this variable surface charge, the affinity of these solids for sorbing most cationic metals at low pH values, like those in Cement Creek, is very low. In contrast, at circum-neutral pH values like those in the Animas River, trace metals are scavenged by Fe, Al and Mn oxide solids (Benjamin and Leckie 1981).

Superimposed on this surface-charge effect, trace metals have an intrinsic affinity for oxide solids as well, and this affinity varies among the oxide solids. For example, Cu and Zn have been reported to have greater affinities for Al oxides than for Fe oxides, but Pb sorbs to Fe oxides more so than Al oxides (Coston et al. 1995, Karthikeyan et al. 1997). For freshly precipitated amorphous to short-

range ordered $Fe(OH)_3$, similar to the colloids precipitated in the Animas River, at low concentrations of sorbing metals, Benjamin and Leckie have reported relative affinities in the order Pb>Cu>Zn>Cd (Benjamin and Leckie 1981). This ordering is consistent with that reported by Ford et al. for freshly precipitated $Fe(OH)_3$ of Pb>Ni>Mn=Cd (Ford et al. 1997).

While partitioning of trace metals on oxide solids is complex, research has converged toward an internally consistent modeling approach to account for both the intrinsic affinity and electrostatic components of the phenomenon. Particularly relevant for the Gold King release, Dzombak and Morel (Dzombak and Morel 1990) have consolidated numerous studies on the sorption of metals on amorphous Fe oxide over a range of pH values and trace-metal concentrations as described by:

$$K_e = \left\{\frac{(SOMe^+)(H^+)}{(SOH)(Me^{2+})}\right\} exp\left(\frac{-zF\Psi_o}{RT}\right) \quad (10)$$

where K_e is a sorption constant, $(SOMe^+)$ is the activity of metal Me^{2+} on the oxide solid surface (molar), (SOH) is the activity of protonated surface species (molar), (Me^{2+}) is the trace metal activity in bulk solution (molar), z is the elementary electrostatic charge of the ion (2 in this example), Ψ_o is the difference in electrostatic potential between the sorption layer and the bulk liquid, a function of deviation of pH from ZPC (V), F is the Faraday Constant (96,485 J/(V mol)), R is the Universal Gas Constant (8.314 J/(K mol)) and T is temperature (K). The equilibrium concentration of metals can be determined by manipulating Equation 10 and transposing (Me) and K_e (Appendix 3). Values for the chemical component of Equation 10 necessary to estimate dissolved concentrations of As, Cu, Pb and Zn in sorptive equilibrium with specified concentrations of ferrihydrite, are summarized from Dzombak and Morel (Dzombak and Morel 1990) in Bethke (Bethke 1998). Values for the electrostatic component of Equation 10 can be determined from graphs and tables reported in Dzombak and Morel. Using total concentration data for four locations in the lower Animas and variables quantitated with Equation 10, dissolved concentrations of As, Cu, Pb and Zn are estimated and compared to observed dissolved concentrations in Table 5. Looking at the "Modeled/Peak Dissolved Ratios" in Table 6, the modeled dissolved cations agree with the observed values at all four river locations as they should considering that dissolved values are used to solve for sorption site density in Equation 10 (Appendix 3). In contrast, this model predicts higher concentrations of the oxyanion AsO_4^- than are reported for these river locations. This probably is due at least partially to having modeled sorption on only one of three As-sorption sites. Some of the deviation might also be due to As binding to Al-oxide colloids, or another phase. Fortunately, the observed values of dissolved As are very low (Table 6), even less than the low values predicted by this sorption-modeling effort.

Mineral recrystallization to more stable phases and the long-term occlusion of trace elements: As oxide solids age, they undergo crystallization to more thermodynamically stable forms (Figure 5), a process commonly called Ostwald ripening (Steefel and van Cappellen 1990). For Fe oxide solids, freshly precipitated amorphous $Fe(OH)_3$ will order itself to short-range ordered $Fe(OH)_3$, then to longer-range order to form the mineral ferrihydrite ($Fe(OH)_3$), and then to still more stable mineral phases such as goethite and hematite (Figure 15). Likewise, as freshly precipitated Al oxides age, they undergo recrystallization from amorphous → microcrystalline → crystalline gibbsite (Figure 16). As these Fe and Al minerals age and recrystallize to more stable phases, they equilibrate with progressively lower solution activities (Nordstrom et al. 1984). These aged mineral phases are widely distributed in soils and sediments, in contaminated and pristine settings alike, throughout the environment.

667 Typical times for recrystallization and growth of selected authigenic Al and Fe oxides, as well as
668 typical particle sizes, have been culled from the literature (Nordstrom et al. 1984, Hsu 1989,
669 Schwertmann and Taylor 1989, Langmuir 1997, Schwertmann and Cornell 2000, Cornell and
670 Schwertmann 2003, Kukkadapu et al. 2003) and summarized in Table 5. Particle sizes listed in
671 Table 5 start with single-grain for incipient nucleation and then flocs/aggregates, as this is the habit
672 for these minerals (Hsu 1989, Schwertmann and Taylor 1989). Particle density of these minerals
673 will fall in the range of 3.9 g/cm^3 (Schwertmann and Taylor 1989). The aggregates listed in Table 5
674 might have considerably lower bulk densities than this value for the amorphous phases but will
675 approach the particle density value as aging occurs and mineral grains inter-grow and become
676 progressively more intimately inter-connected.

677 The rate at which these colloids settle from the water column will not be a function solely of density
678 and particle size, but also surface charge and concentrations of counter-ions in solution. Surface
679 charge is a function of pH; the further pH is from the zero-point-of-charge (ZPC), the greater the
680 surface charge. Oxide minerals of Al and Fe generally have ZPCs of 8 and higher (Table 5). For an
681 upper Animas pH of ~6.5 to ~7.5 then, these colloids would have been mildly positively charged and
682 relatively high concentrations of divalent $SO_4^=$ would have enhanced flocculation, aggregation and
683 settling. In the lower Animas, pH generally is ~8.3, decreasing surface charge on these colloids.
684 Coupled with possibly lower $SO_4^=$ in the lower Animas due to dilution and higher concentrations of
685 monovalent HCO_3^- from carbonate dissolution, colloid flocculation might have been less effective in
686 the lower Animas, perhaps fostering suspended transport in the water column.

687 As incipient mineral solids age to stable crystalline minerals, progressively larger fractions of trace
688 metals in these minerals become bound nonreversibly or hysterically (Ford et al. 1997). As these
689 solids crystallize and recrystallize, their relative affinities for metals changes but overall the
690 reversibility of metal binding continues to diminish (Coughlin and Stone 1995). For example, Ford
691 et al. noted that, as the $Fe(OH)_3$ aged, affinity of the solid for Mn and Ni increased, but the affinity
692 for Pb and Cd decreased (Ford et al. 1997). And the relative affinities of thermodynamically stable
693 minerals for sorbing metals varies from that of $Fe(OH)_3$ as well. For example, Forbes et al. (Forbes
694 et al. 1976) reported relative affinities for goethite as Cu>Pb>Zn>Co>Cd which is consistent with
695 that reported by Coughlin and Stone (Coughlin and Stone 1995), Cu>Pb>Ni=Co>Mn. As a result of
696 this long-term recrystallization to more stable thermodynamic minerals, and concomitant hysteric
697 binding of trace metals, the long-term fate of much of the released trace metals is to be bound in the
698 lattices of stable Fe and Al oxide minerals.

699

700 **Placing the release in context of long-term releases from Gold King and similar mines:** Over
701 the long term, all mines discharge water at the same rate that they are recharged. The minimum rate
702 of recharge to a mine generally is determined by the (i) regional groundwater recharge rate, (ii) area
703 of the mine and (iii) depth of the mine. Sometimes, nearby mines might divert recharge away from a
704 neighboring mine that otherwise would enter the mine or increase recharge to the mine, effectively
705 decreasing or increasing the mine's footprint. And sometimes, if a mine approaches a surface water
706 body, excess water might leak into the mine. Barring complicating factors, however, recharge to
707 mines can be reasonably estimated from information on precipitation-recharge rate, mine area and
708 mine depth alone.

709 For abandoned mines, often the largest part of discharge commonly is not visible as discrete
710 surface flow, instead winnowing its way to the surface at numerous small stream-bank weeps and as
711 diffuse stream-bottom discharge. According to the owner of Gold King Mine, at one time the main
712 discrete discharge from Gold King was 7 gallons per minute (gpm) (Castillo 2015). The owner
713 reports that, when hydrologic practices changed in an adjacent mine (e.g., installing bulkheads in the

American Tunnel), the main discrete discharge from Gold King increased to 250 gpm (950 liters/minute) (Castillo 2015). A rate of 250 gpm roughly equates to 1.4M liters per day, roughly 12% of the estimated August 5 release volume of 11M liters. So at the recent rate of discharge, the volume of the Gold King release was being released from Gold King Mine every eight days.

Put in this context, given normal variability of environmental systems, the contamination released by the Gold King Mine breach was not fated to be vaulted away for centuries, but would have been expected to have residence times in the mine of days or weeks before discharge to Cement Creek.

Analytical considerations

1) When characterizing mining discharges, always measure pH (in the field) and dissolved Fe^{2+}, Fe^{3+}, Al^{3+} and Mn^{2+} so that acidity can be calculated. Acidity characterizes the AMD capacity to maintain acidic pH values, conditions under which toxic-metal mobility is high. Knowledge of iron valence not only is necessary for calculating acidity, but also affects rates at which acidity releases free H^{+}, thereby dropping pH. Also knowledge of Fe valence allows calculation of the potential for precipitation or dissolution of ferric and ferrous minerals.

2) When characterizing mining discharges, measure $SO_4^{=}$ so that ionic strength, activity coefficients and complexation can be calculated easily.

3) When there is an AMD release, and knowledge of the fate of the release metals is desired, collect samples of the streambed upgradient (for background) and downgradient to below where the AMD staining (e.g., "yellowboy") is evident. Consider running two selective extractions on these sediment samples: i) oxalate extraction to characterize incipient oxide minerals and the AMD metals in this phase; and ii) dithionite extraction to characterize the pre-existing authigenic oxide minerals, and their metals, as a reference to gauge the magnitude by which release metals exceed the pre-existing state of the streambed.

4) When characterizing mining discharges, measure acidity in the water phase with a heated pre-oxidation step followed by titration with a base. For example, EPA Method 305.1 is intended for this purpose.

References

Benjamin, M. M. and J. O. Leckie (1981). "Multiple-site adsorption of Cd, Cu, Zn, and Pb on amorphous iron oxyhydroxide." Journal of Colloid and Interface Science **79**: 209-221.

Bethke, C. M. (1998). The Geochemist's Workbench, Release 3.0. Urbana-Champaign, IL, U. Illinois.

Bigham, J. M. and D. K. Nordstrom (2000). "Iron and aluminum hydroxysulfates from acid sulfate waters." Reviews in Mineralogy and Geochemistry **40**: 351-403.

Bigham, J. M., U. Schwertmann and G. Pfab (1996). "Influence of pH on mineral speciation in a bioreactor simulating acid mine drainage." Applied Geochemistry **11**: 845-849.

Bigham, J. M., U. Schwertmann, S. J. Traina, R. L. Winland and M. Wolf (1996). "Schwertmannite and the chemical modeling of iron in acid sulfate waters." Geochimica et Cosmochimica Acta **60**: 2111-2121.

Brophy, G. P. and M. F. Sheridan (1965). "Sulfate Studies IV: the jarosite-natrojarosite-hydronium jarosite solid solution series." The American Mineralogist **50**: 1595-1607.

Castillo, M. (2015). Gold King Mine Owner: 'I foresaw disaster' before spill. CNN website: http://www.cnn.com/2015/08/13/us/colorado-epa-animas-river-spill-owner/index.html.

Church, S. E., P. von Guerard and S. E. Finger (2007). Integrated investigation of environmental effects of historical mining in the Animas River watershed, San Juan County, Colorado. E5. Mine inventory and compilation of mine-adit chemistry data. , US Geological Survey.

Cornell, R. M. and U. Schwertmann (2003). The Iron Oxides. Darmstadt, Germany, Wiley-VCH.

Coston, J. A., C. C. Fuller and J. A. Davis (1995). "Pb nad Zn adsorption by a natural aluminum- and iron-bearing surface coating on an aquifer sand." Geochimica et Cosmochimica Acta **59**: 3535-3547.

Coughlin, B. R. and A. T. Stone (1995). "Nonreversible adsorption of divalent metal ions (Mn, Co, Ni, Cu, and Pb) onto goethite: effects of acidification, Fe addition, and picolinic acid addition." Environmental Science & Technology **29**: 2445-2455.

Desborough, G. A. and D. B. Yager (2000). Acid-neutralizing potential of igneous bedrocks in the Animas Riveer headwaters, San Juan County, Colorado. U. S. G. Survey.

Dzombak, D. A. and F. M. M. Morel (1990). Surface Complex Modeling: Hydrous Ferric Oxide. New York, NY, John Wiley & Sons.

Forbes, E. A., A. M. Posner and J. P. Quirk (1976). "The specific adsorption of divalent Cd, Co, Cu, Pb, and Zn on goethite." Journal of Soil Science **27**: 154-166.

Ford, R. G., P. M. Bertsch and K. J. Farley (1997). "Changes in transition and heavy metal partitioning during hydrous iron oxide aging." Environmental Science & Technology **31**: 2028-2033.

Gobla, M. J. and C. M. Gemperline (2015). Technical evaluation of the Gold King Mine incident. Reclamation: Managing Water in the West. Denver, CO, U.S. Department of the Interior, Bureau of Reclamation: 64.

780 Hsu, P. H. (1989). Chapter 7 Aluminum oxides and hydroxides. Minerals in Soil Environments. J. B.
781 Dixon and S. B. Weed. Madison, WI, Soil Science Society of America: 331-378.

782 Karthikeyan, K. G., H. A. Elliott and F. S. Cannon (1997). "Adsorption and coprecipitation of copper
783 with the hydrous oxides of iron and aluminum." Environmental Science & Technology **31**: 2721-
784 2725.

785 Kukkadapu, R. K., J. M. Zachara, J. K. Fredrickson, S. C. Smith, A. C. Dohnalkova and C. K.
786 Russell (2003). "Transformation of 2-line ferrihydrite to 6-line ferrihydrite under oxic and anoxic
787 conditions." American Mineralogist **88**: 1903-1914.

788 Langmuir, D. (1997). Aqueous Environmental Geochemistry. Upper Saddle River, NJ, Prentice Hall.

789 Luedke, R. G. and W. S. Burbank (1999). Geologic map of the Silverton and Howardsville
790 quadrangles, southwestern Colorado. U. S. G. Survey.

791 Nordstrom, D. K. (2011). "Hydrogeochemical processes governing the origin, transport and fate of
792 major and trace elements from mine wastes and mineralized rock to surface waters." Applied
793 Geochemistry **26**: 1777-1791.

794 Nordstrom, D. K., S. D. Valentine, J. W. Ball, L. N. Plummer and B. F. Jones (1984). Partial
795 compilation and revision of basic data in the WATEQ programs. Water-Resources Investigation
796 Report 84-4186. Menlo Park, CA, U.S. Geological Survey: 43.

797 Olivarius-Mcallister, C. (2013). A legacy that won't die. The Durango Herald.
798 http://www.durangoherald.com/article/20130803/NEWS01/130809830/-1/mining/A-legacy-that-
799 won't-die-&template=miningart.

800 Parizek, R. R., W. B. White and D. Langmuir (1971). Hydrogeology and geochemistry of folded and
801 faulted rocks of the central Appalachian type and related land use problems. University Park, PA,
802 Penn State University.

803 Rose, A. W. and C. A. I. Cravotta (1998). Geochemistry of Coal Mine Drainage. Coal Mine
804 Drainage Prediction and Pollution Prevention. Harrisburg, Pennsylvania, Pennsylvania Department
805 of Environmental Protection: 1-1 to 1-22.

806 Rose, A. W., Hawkes, Herbert E., Webb, John S. (1979). Geochemistry in Mineral Exploration, 2nd
807 Edition. New York, NY USA, Academic Press.

808 Schemel, L. E. and M. H. Cox (2005). Descriptions of the Animas River-Cement Creek Confluence
809 and Mixing Zone near Silverton, Colorado, during the Late Summers of 1996 and 1997, U.S.
810 Geological Survey.

811 Schwertmann, U. and R. M. Cornell (2000). Iron Oxides in the Laboratory. New York, NY, Wiley-
812 VCH.

813 Schwertmann, U. and R. M. Taylor (1989). Chapter 8 Iron oxides. Minerals in Soil Environments. J.
814 B. Dixon and S. B. Weed. Madison, WI, Soil Science Society of America: 380-438.

815 Scott, K. M. (1987). "Solid solution in, and classification of, gossan-derived members of the alunite-
816 jarosite family, northwest Queensland, Australia." The American Mineralogist **72**: 178-187.

817 Singer, P. C. and W. Stumm (1970). "Acidic mine drainage: The rate-determining step." Science
818 **167**: 1121-1123.

819 Skousen, J., A. W. Rose, G. Geidel, J. Foreman, R. Evans and W. Hellier (1998). A Handbook of
820 Technologies for Avoidance and Remediation of Acid Mine Drainage. Morgantown, WV, The
821 National Mine Land Reclamation Center, West Virginia University: 131.

822 Steefel, C. I. and P. V. van Cappellen (1990). "A new kinetic approach to modeling water-rock
823 interaction: the role of nucleation, precursors, and Ostwald ripening." Geochimica Et Cosmochimica
824 Acta **54**(10): 2657-2677.

825 Stumm, W. and W. W. Morgan (1981). Aquatic Chemistry. New York, NY, Wiley-Interscience.

826 Sverjensky, D. A. (1994). "Zero-point-of-charge prediction from crystal chemistry and solvation
827 theory." Geochimica Et Cosmochimica Acta **58**: 3123-3129.

828 U.S.G.S. (1982). 1:100000-scale metric topographic map of Silverton, CO. 30x60 Minute Series.
829 Reston, VA, U.S. Geological Survey.

830 US-Mining. (2016). "San Juan County, CO Mines. http://www.us-mining.com/colorado/san-juan-
831 county."

832 Washington, J. W., D. M. Endale, L. P. Samarkina and K. E. Chappell (2004). "Kinetic control of
833 oxidation state at thermodynamically buffered potentials in subsurface waters." Geochimica Et
834 Cosmochimica Acta **68**: 4831-4842.

835 Yager, B. B. and D. J. Bove (2002). Generalized geologic map of part of the upper Animas River
836 watershed and vicinity, Silverton, Colorado, U.S. Geological Survey.

837 Yager, D. B., A. M. Mast, P. L. Verplanck, D. J. Bove, W. G. Wright and P. L. Hagerman (2000).
838 Natural Versus Mining-Related Water Quality Degradation to Tributaries Draining Mount Moly,
839 Silverton, Colorado. Fifth International Conference on Acid Rock Drainage (ICARD2000), Denver,
840 CO, Society for Mining, Metallurgy, and Exploration, Inc.

841 Youtube. (2015). "EPA releases Gold King Mine blowout footage:
842 https://www.youtube.com/watch?v=ZBlR05tDCbI."

843

844

Appendix 1: Fe^{2+} oxidation kinetics of Singer and Stumm

Singer and Stumm (1970) report the abiotic oxidation of Fe^{2+} in water by dissolved O_2 to proceed at a rate according to:

$$\frac{-d[Fe^{2+}]}{dt} = k[Fe^{2+}][O_2][OH^-]^2 + k'[Fe^{2+}][O_2] \quad (1)$$

Rearranging:

$$\frac{d[Fe^{2+}]}{[Fe^{2+}]} = -\{k[O_2][OH^-]^2 + k'[O_2]\}dt \quad (2)$$

Integrating:

$$\int \frac{d[Fe^{2+}]}{[Fe^{2+}]} = -\{k[O_2][OH^-]^2 + k'[O_2]\} \int dt \quad (3)$$

$$ln\frac{[Fe^{2+}]_t}{[Fe^{2+}]_0} = -[O_2]\{k[OH^-]^2 + k'\}\Delta t \quad (4)$$

Rearranging and solving for half-life:

$$T_{1/2} = \frac{\ln 2}{[O_2]\{k[OH^-]^2 + k'\}} \quad (5)$$

Singer and Stumm (1970) report values of k and k", [OH-] is specified by designating pH, and [O2] is taken as in equilibrium with the atmosphere, 0.208 atmospheres.

Appendix 2: Reactions and equations for calculating calcite and dolomite saturation

For calcite reacting with water:

$$CaCO_3 + 2a_{H^+} \leftrightarrow a_{Ca^{2+}} + f_{CO_2} + a_{H_2O} \quad (1)$$

where $CaCO_3$ is calcite, a is activity and f is fugacity. Measures of pH are measures of H+ activity, a_{H^+} = -log (pH). Activity of other solutes is calculated from concentration by multiplying concentration by the activity coefficient γ. The value of γ is calculated from the extended Debye-Huckel equation (Stumm and Morgan 1981). Likewise *f* is calculated from partial pressure multiplying partial pressure by the fugacity coefficient; for these calculations, the fugacity coefficient is taken as unity. In these calculations P_{CO2} is taken as $10^{-3.4}$ atmospheres, the August 2015 monthly mean CO_2 partial pressure recorded at the NOAA, Mauna Loa, HI observatory (http://www.esrl.noaa.gov/gmd/ccgg/trends/). Using the thermodynamic data reported in Parizek et al. (1971), log K for Reaction 1 is -9.86. Then the saturation index for calcite, $SI_{calcite}$ is:

$$SI_{calcite} = \log\left\{\frac{a_{Ca^+} f_{CO_2}}{a_{H^+}^2 \, 10^{9.86}}\right\} \quad (2)$$

By analogy with calcite, the governing equations for dolomite saturation are:

$$CaMg(CO_3)_2 + 4a_{H^+} \leftrightarrow a_{Ca^{2+}} + a_{Mg^2} + 2f_{CO_2} + 2a_{H_2O} \quad (3)$$

where $CaMg(CO_3)_2$ is dolomite and log K = -19.71. Then:

$$SI_{dolomite} = \log\left\{\frac{a_{Ca^+} a_{Mg^{2+}} 2f_{CO_2}^2}{a_{H^+}^4 \, 10^{19.71}}\right\} \quad (4)$$

Appendix 3: Solving for dissolved metals in equilibrium with $Fe(OH)_3$ colloids

Using Zn^{2+} at Durango as an example:

$$Log\ K_{strong} + \frac{zF\Psi}{RT} = Log\ K_{app} = -0.96 \quad (1)$$

$$K_{app} = 10^{-0.96} = \frac{a_{Zn^{2+}}[>FeOH]}{a_{H^+}[>FeOZn^+]} \quad (2)$$

The variables a_{Zn2+} and a_{H+} are measured.

Assuming sorbing metals do not interfere with one another,

$$[>FeTot] = [>FeOH] + [>FeOZn^+] \quad (3)$$

Where [>FeTot] represents the total concentration of potential sorption sites for Zn^{2+}, both unoccupied and occupied. Dzombak and Morel offer a method to calculate [>FeTot] from values of total Zn concentration in water samples. Rearranging Eqtn 3 and substituting into Eqtn 2:

$$K_{app} = 10^{-0.96} = \frac{a_{Zn^{2+}}[>FeOH]}{a_{H^+}([>FeTot]-[FeOH])} \quad (4)$$

$$[>FeOH] = \frac{10^{-0.96}a_{H^+}([>FeTot]-[>FeOH])}{a_{Zn^{2+}}} \quad (5)$$

$$[>FeOH] + \frac{10^{-0.96}a_{H^+}[>FeOH]}{a_{Zn^{2+}}} = \frac{10^{-0.96}a_{H^+}[>FeTot]}{a_{Zn^{2+}}} \quad (6)$$

$$[>FeOH]\left\{1 + \frac{10^{-0.96}a_{H^+}}{a_{Zn^{2+}}}\right\} = \frac{10^{-0.96}a_{H^+}[>FeTot]}{a_{Zn^{2+}}} \quad (7)$$

$$[>FeOH] = \frac{10^{-0.96}a_{H^+}[>FeTot]}{a_{Zn^{2+}} + (10^{-0.96})a_{H^+}} \quad (8)$$

Then [>FeOZn$^+$] can be determined by substituting Eqtn 8 into Eqtn 3 and rearranging.

922

923

924 **Figure C-1. Location of Gold King Mine, north of Silverton, in the Cement Creek watershed. Image**
925 **from USGS, 30x60 Silverton, Colorado Quad (U.S.G.S. 1982). Water flow is north to south.**
926 **Animas River flows NNE to SSW, with Silverton situated on its western bank. Cement Creek flows**
927 **from north of Gold King Mine to its confluence with the Animas just north of Silverton. Mineral**
928 **Creek flows from the west to its confluence with the Animas just south of Silverton.**

929

930

931

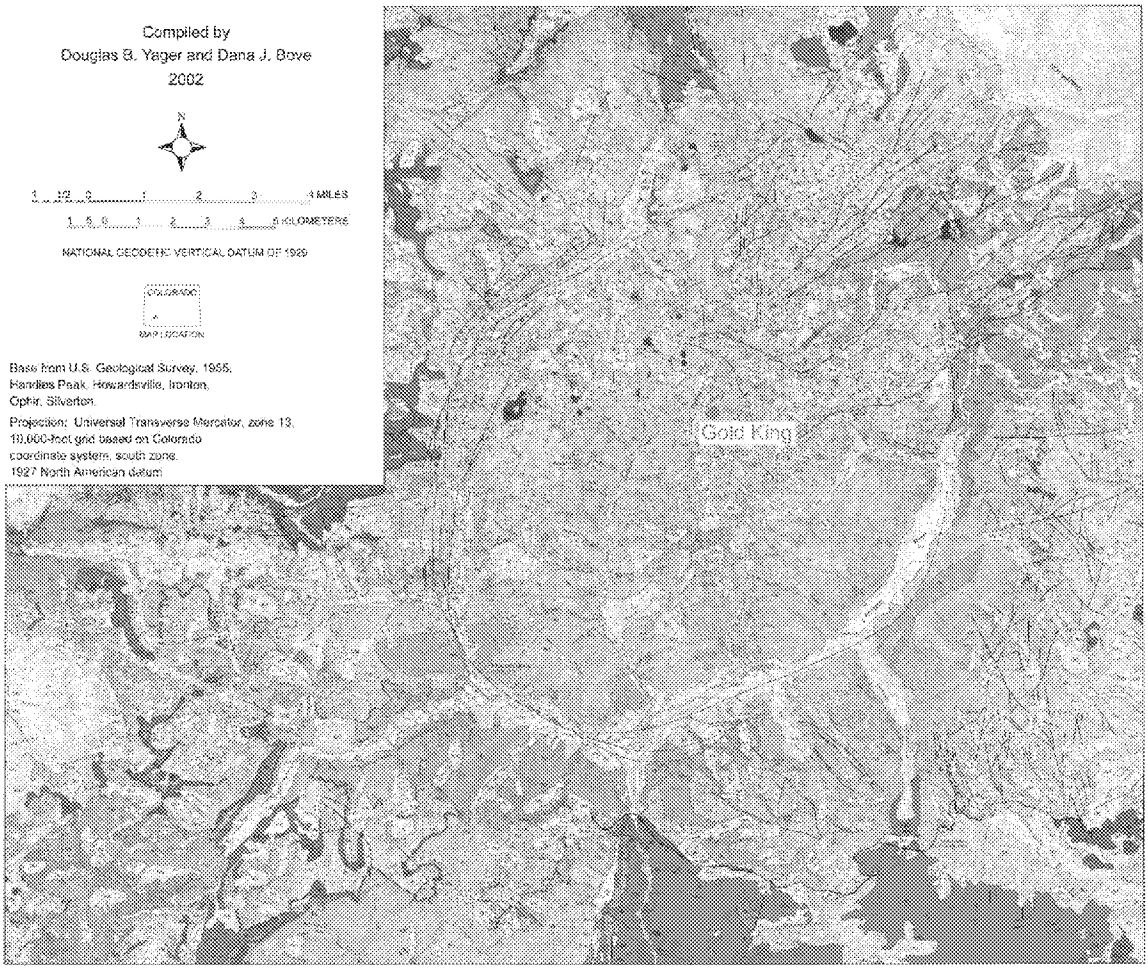

932

933 **Figure C-2. Geologic map of the area surrounding Gold King Mine. Mapping units are lost in this image**
934 **because it is reduced from the original scale. However, the outline of Silverton Caldera in which Gold King**
935 **Mine is situated is clearly visible, bounded by the Animas River to the east, Mineral Creek to the south,**
936 **and outlined by sub-parallel sets of faults and vein structures (black lines) to the west and northwest.**
937 **This view shows that Cement Creek drains the highly mineralized Silverton Caldera exclusively. Original**
938 **map is by Yager and Bove (Yager and Bove 2002). The volcanic release from this caldera was 75 km^3, a**
939 **volume much in excess of the 1980 release from Mt. St. Helens of 0.5 km^3, for comparison (Doug Yager,**
940 **USGS, personal communication to John Washington, USEPA, May 10, 2016).**

941

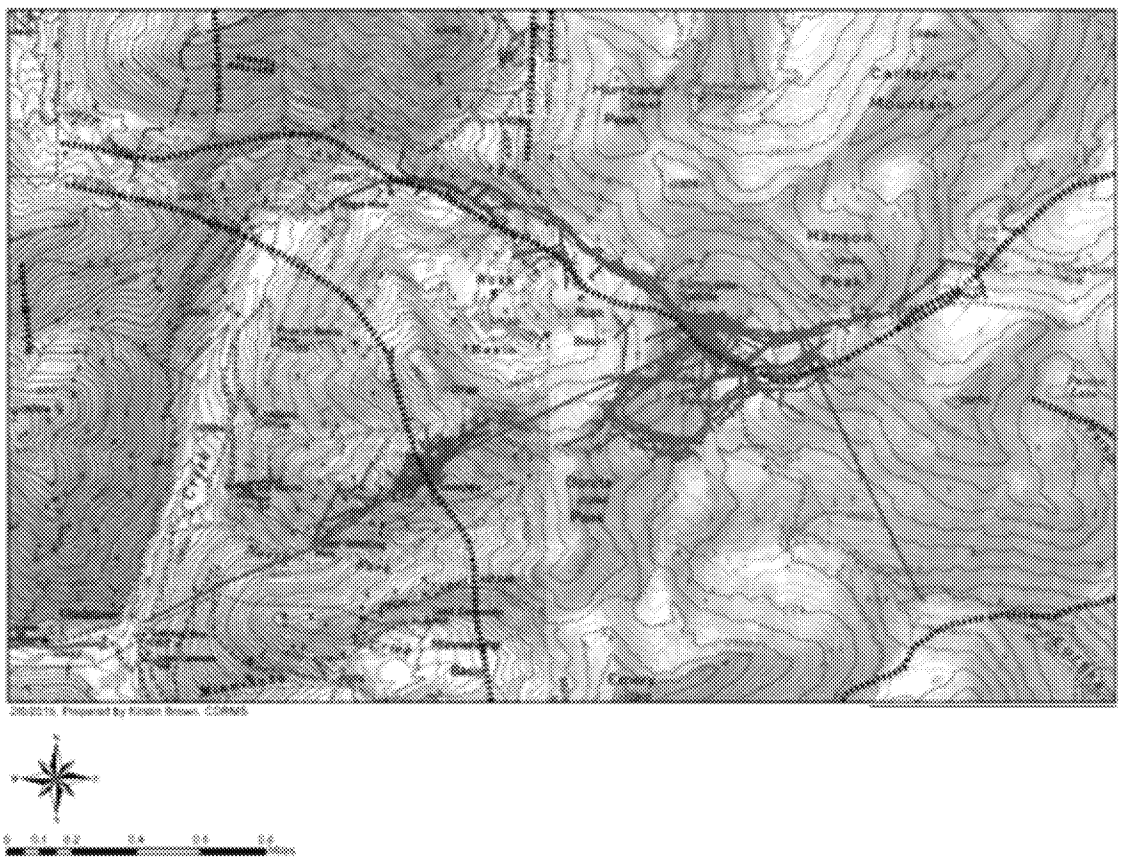

942

943

944 **Figure C-3. Map depicting footprints for Gold King Mine (pink), Red and Bonita Mine (red), Mogul and**
945 **Grand Mogul Mines (blue), and Sunnyside Mine (green) with the American Tunnel (also green) extending**
946 **westerly under Gold King to emerge near Gladstone. Map is from Gobla and Gemperline (Gobla and**
947 **Gemperline 2015).**

948

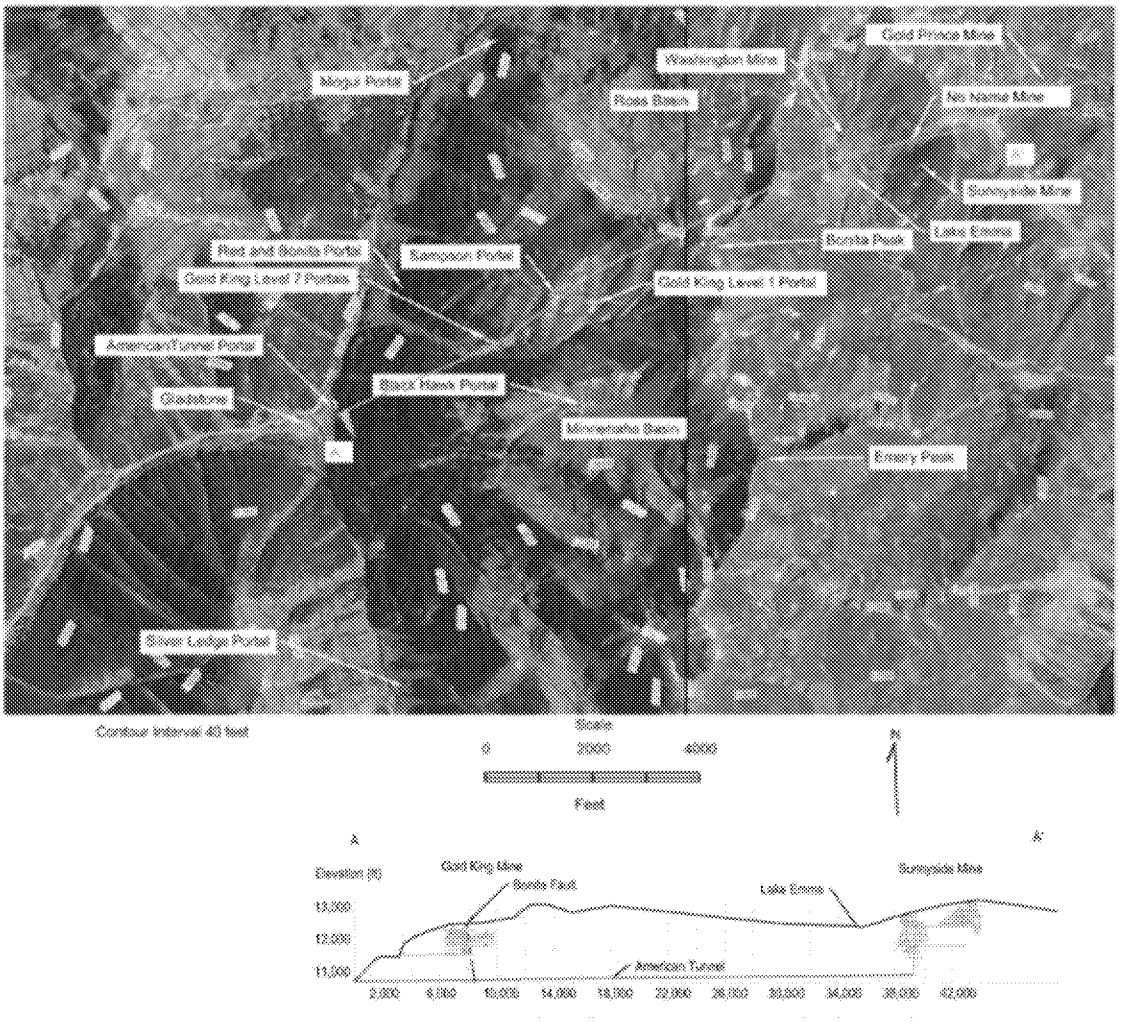

Figure C-4. Aerial trace and profile of a cross-section through Sunnyside and Gold King mines. This profile illustrates that Sunnyside Mine can drain through the American Tunnel, under Gold King Mine. The Bonita fault bisects Gold King Mine and the American Tunnel, likely fostering hydraulic connectivity between the mines. Lake Emma, located west of Sunnyside Mine on the cross-section, is reported to have failed and drained into the Sunnyside complex in 1978 . Images are from Gobla and Gemperline (Gobla and Gemperline 2015).

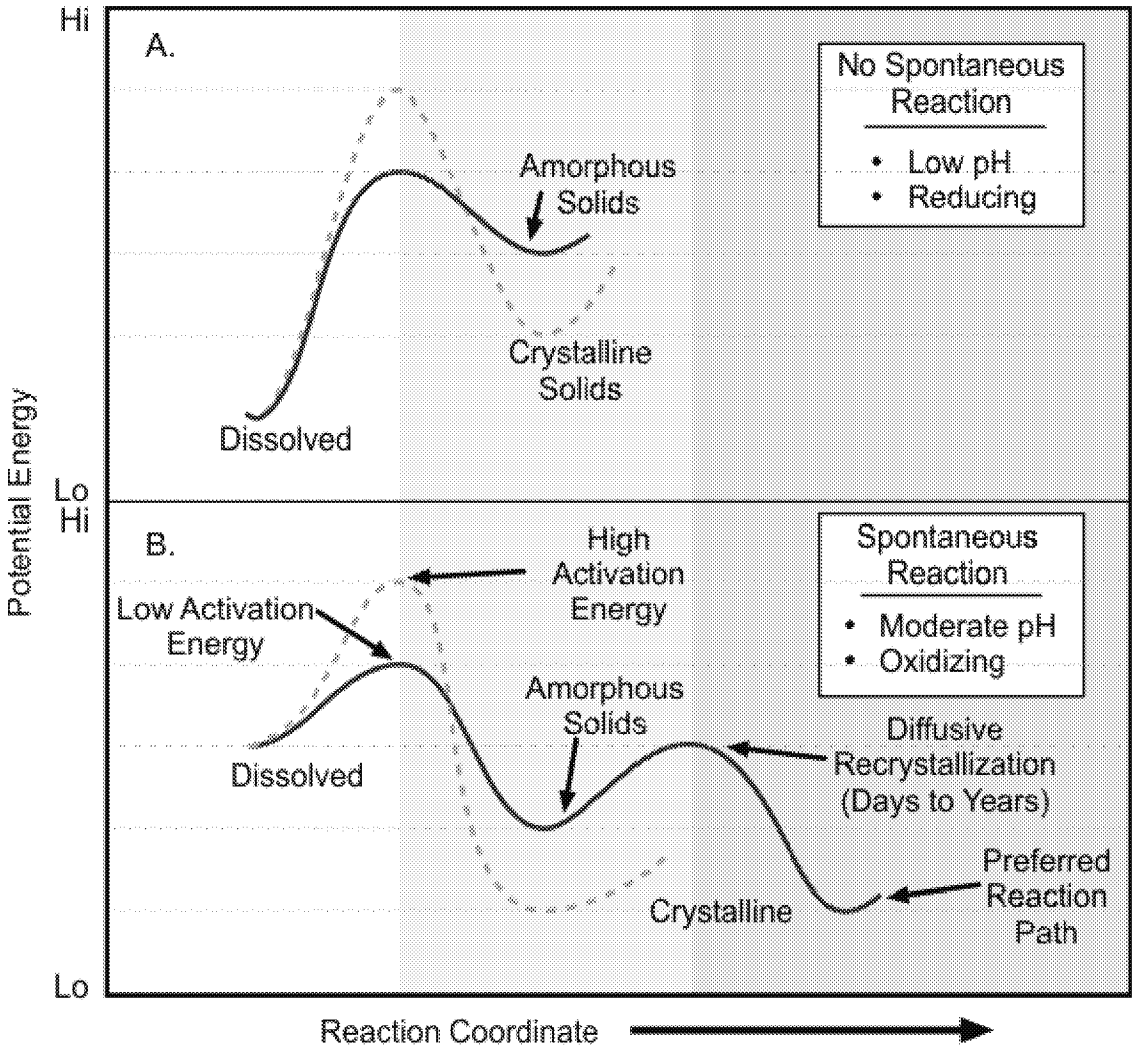

957

958 **Figure C-5. Potential energy (for which low energy is relatively stable) vs reaction progress. Under**
959 **conditions expected in a deep subsurface minepool, metals largely are stable in the dissolved state (A).**
960 **When mine waters are released to common surficial conditions (moderate pHs and oxidizing), Fe, Al and**
961 **Mn generally nucleate and precipitate to form amorphous or short-ranged ordered oxide minerals (e.g.,**
962 **ferrihydrite, gibbsite, birnessite) that are prominent in AMD releases as "yellowboy," but these solids**
963 **slowly recrystallize to more stable crystalline phases (e.g., hematite, goethite, and ordered gibbsite and**
964 **birnessite).**

965

966

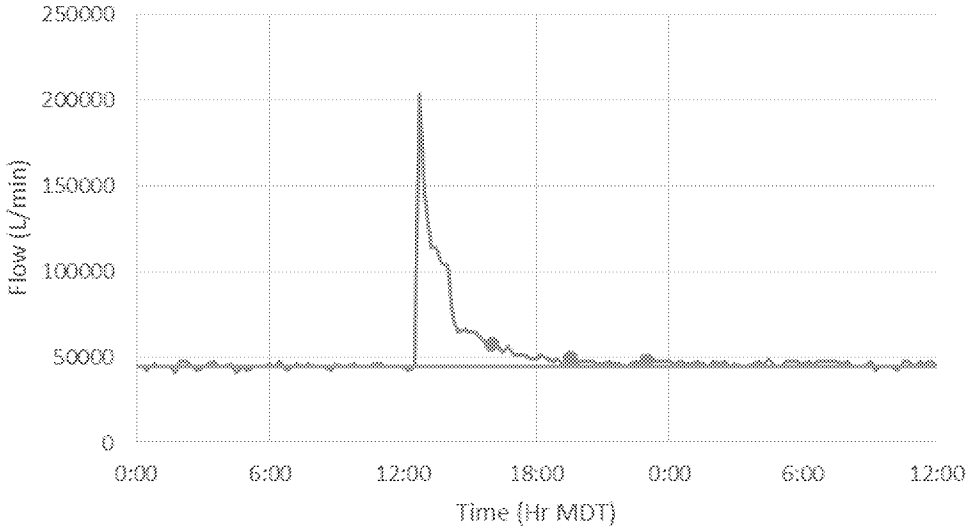

967

968 **Figure C-6. Hydrograph at gage CC48 on Cement Creek, for August 5, 2015. The horizontal line is the**
969 **average of the flow values prior to arrival of the mine release waters. The orange points designate when**
970 **a sample was collected from nearby 14th St Bridge or at CC48 for chemical analysis.**

971

Table C-1. Samples useful for characterizing release-water composition.

Study Location		CC06 Discharge		GKM13 Cement Creek		CC 14th St Bridge Cement Creek	
Site Location							
Sample Date		8/15/2015		8/15/2015		8/5/2015	
Sample Time		9:00		10:45		16:00	
Distance from source	(km)	0		0.87		13.46	
		Dissolved	Total	Dissolved	Total	Dissolved	Total
pH	(SU)	2.93	2.93	3.19	3.19		
Aluminum	(mg/l)	34	33	28	26	91.9	945
Antimony	(mg/l)	0.0037	0.00062	0.0015	0.0004	0	0.321
Arsenic	(mg/l)	0.044	0.0055	0.016	0.0012	0	8.23
Barium	(mg/l)	0.0086	0.0087	0.0085	0.009	0	9.73
Beryllium	(mg/l)	0.011	0.011	0.009	0.0086	0.0348	0.135
Cadmium	(mg/l)	0.082	0.085	0.08	0.084	0.0983	0.165
Calcium	(mg/l)	370	380	350	360	461	454
Chromium	(mg/l)	0.0055	0.003	0.0033	0.001	0	0.706
Cobalt	(mg/l)	0.11	0.11	0.1	0.1	0.204	0.384
Copper	(mg/l)	4.6	4.6	3.9	3.8	10.4	36.7
Iron	(mg/l)	150	120	96	70	49.5	9930
Lead	(mg/l)	0.042	0.029	0.024	0.011	0.15	179
Magnesium	(mg/l)	27	27	26	28	36.5	279
Manganese	(mg/l)	36	36	31	32	37.1	78
Mercury	(mg/l)	0.00008	0.00008	0.00008	0.00008		0.0192
Molybdenum	(mg/l)	0.0042	0.00077	0.0014	0.00045	0	2.01
Nickel	(mg/l)	0.069	0.072	0.068	0.07	0.0915	0.276
Potassium	(mg/l)	2.4	2.5	2.2	2.2	6.63	212
Selenium	(mg/l)	0.0047	0.0033	0.0038	0.0032	0	0
Silver	(mg/l)	0.0001	0.0001	0.0001	0.0001	0	1.11
Sodium	(mg/l)	5.3	5.2	52	54	4.96	23.4
Thallium	(mg/l)	0.00029	0.00029	0.00023	0.00023	0	0
Vanadium	(mg/l)	0.038	0.0025	0.014	0.0003	0	5.47
Zinc	(mg/l)	20	20	18	18	26.8	44
Sulfate	(mg/l)	1600	1600	1400	1400		
Chloride	(mg/l)	0.36	0.36	1.2	1.2		
Fluoride	(mg/l)	10	10	8.9	8.9		
Nitrate as N	(mg/l)	0.023	0.023	0.025	0.025		

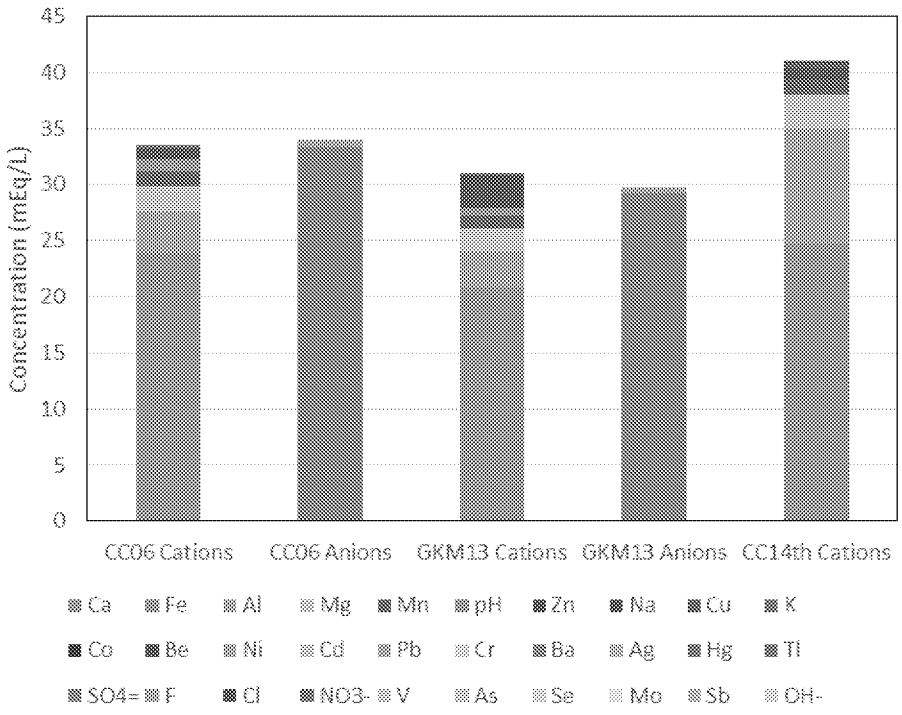

975

976 **Figure C-7. Cation/anion balance for water samples from CC06, GKM13, and CC14th Street Bridge.**
977 **Cation/anion for CC06 is 0.986 and for GKM13 is 1.043, close to the ideal balance of 1.000. Anions and pH**
978 **were not analyzed for the CC14th St sample. The valence of Fe was not analyzed. However, at pH~3, the**
979 **dominant species of ferrous Fe is Fe^{2+} and of ferric Fe is as $FeOH^{2+}$ (neglecting $SO_4^{=}$), so Fe is represented**
980 **here as having 2+ charge.**

981

982 **Table C-2. Conservative estimate of composition of release waters that flowed from Cement Creek into**
983 **the Animas River.**

Analyte	Dissolved Concentration					Dissolved Load			
	Unit	Peak Flow at 12:45 PM	Plume + Bkgnd Mean	Creek Bkgnd	Plume Mean	Unit	Plume + Bkgnd	Bkgnd During Plume	Plume Only
Aluminum	mg/l	619	113	7.60	542	kg	6541	352.6	6188
Antimony	mg/l	0.015	0.003	0.000	0.015	kg	0.194	0.019	0.176
Arsenic	mg/l	0.301	0.051	0.005	0.238	kg	2.95	0.237	2.71
Barium	mg/l	0.069	0.025	0.015	0.067	kg	1.46	0.696	0.769
Beryllium	mg/l	0.231	0.042	0.002	0.205	kg	2.42	0.077	2.35
Cadmium	mg/l	0.674	0.125	0.010	0.594	kg	7.23	0.447	6.78
Calcium	mg/l	2438	537	177	2003	kg	31073	8195	22878
Chromium	mg/l	0.006	0.004	0.001	0.014	kg	0.207	0.046	0.161
Cobalt	mg/l	1.26	0.24	0.03	1.11	kg	13.9	1.24	12.6
Copper	mg/l	70.92	12.6	0.40	62.4	kg	731	18.56	712.6
Iron	mg/l	268	61	13.3	255	kg	3528	619	2910
Lead	mg/l	1.03	0.20	0.02	0.93	kg	11.8	1.14	10.61
Magnesium	mg/l	197	43	9.93	175	kg	2462	461	2001
Manganese	mg/l	206	41	5.80	185	kg	2385	269	2116
Mercury	mg/l	0.000	0.000	0.000	0.000	kg	0.004	0.004	0.000
Molybdenum	mg/l	0.025	0.006	0.000	0.028	kg	0.345	0.023	0.322
Nickel	mg/l	0.55	0.11	0.02	0.46	kg	6.15	0.88	5.27
Potassium	mg/l	40.6	8.0	1.77	33.3	kg	462	82.0	380
Selenium	mg/l	0.034	0.007	0.001	0.034	kg	0.415	0.027	0.388
Silver	mg/l	0.017	0.004	0.000	0.017	kg	0.204	0.005	0.200
Sodium	mg/l	18.0	5.9	4.40	12.0	kg	341	204	137
Thallium	mg/l	0.016	0.003	0.000	0.017	kg	0.202	0.009	0.194
Vanadium	mg/l	0.064	0.014	0.003	0.058	kg	0.800	0.138	0.662
Zinc	mg/l	157	31	3.00	145	kg	1790	139	1651
Sulfate	mg/l	11240	2386	613	9588	kg	137949	28449	109500
pH	SU	2.90	2.90	2.90	2.90	kg	73.4	58.9	14.5
Acidity	$mgCaCO_3/l$	4598	931	152	4097	kg $CaCO_3$	53822	7031	46791

984

985

986

Table C-3. Abiotic Fe^{2+} oxidation half-life at P_{O2} = 0.2 atm. calculated as a function of pH, using kinetic data of Singer and Stumm

pH (su)	$T_{1/2}$
0	65.89 years
1	65.89 years
2	65.64 years
3	61.01 years
4	7.32 years
5	30.05 days
6	7.22 hours
7	4.33 minutes
8	2.60 seconds
9	0.03 seconds

Explanation: In Cement Creek, pH probably ranged from 2 to 4 (red field), so abiotic Fe^{2+}-oxidation half-life likely was years to decades, effectively yielding no ferric Fe during the hours-long transit from Gold King Mine down Cement Creek to the Animas River. In the Animas River, pH likely dominantly ranged from 6 to 8 (green field), so abiotic Fe^{2+} oxidation half-life likely was seconds to hours, and probably mostly in the seconds to minutes range shortly after the release waters mixed with the Animas water. Consequently, Fe^{2+} in the release waters likely oxidized to Fe^{3+} quickly in the Animas River.

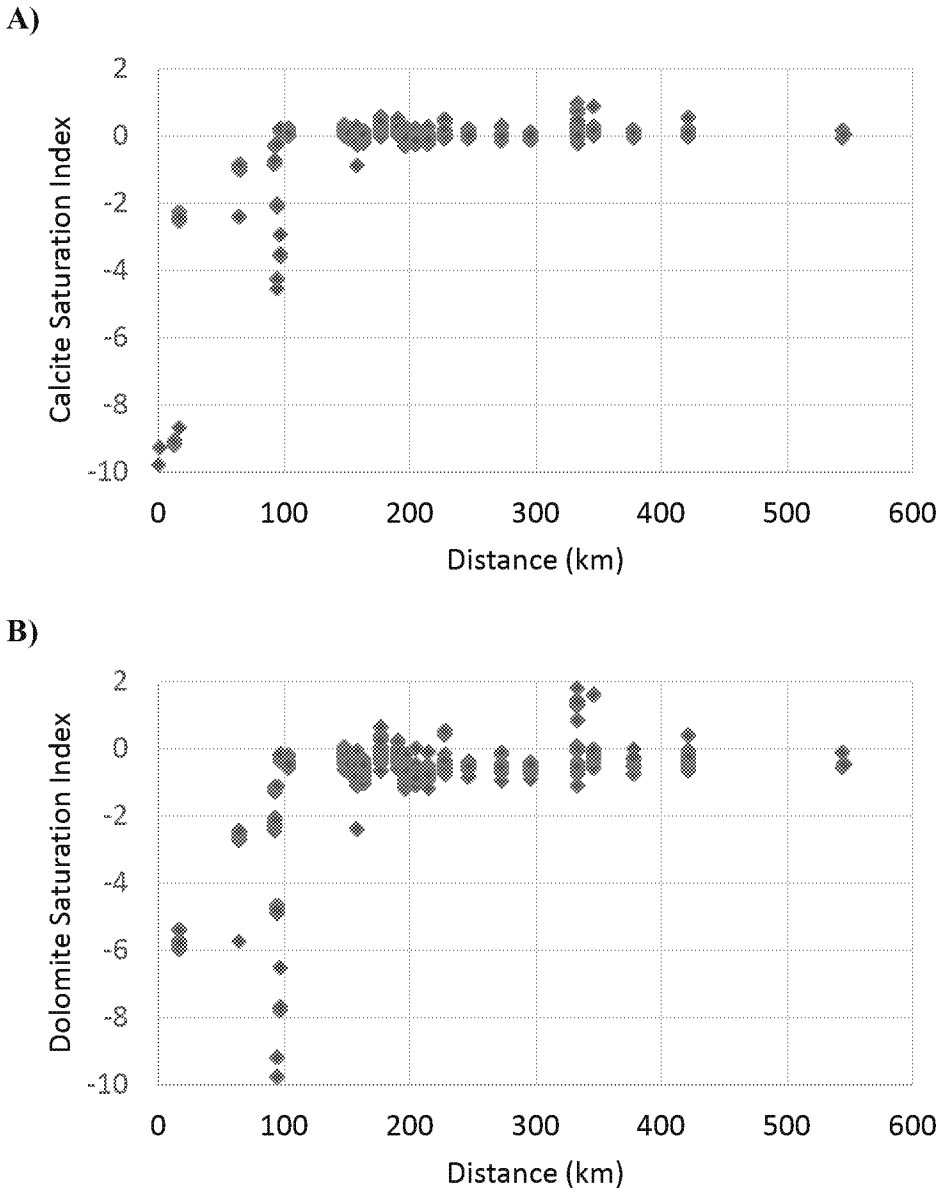

998 **Figure C-8. Saturation Indices (SIs) for calcite (A) and dolomite (B) vs distance from Gold King Mine. An SI**
999 **of zero indicates saturation with the mineral phase. Negative SI values indicates that the water is**
1000 **undersaturated with the mineral.**

1001

1002 **Table C-4. Properties assumed in thermodynamic reaction-progress modeling of plume waters flowing**
1003 **into the Animas River**

Parameter	Assignation
Temperature	11 °C
O_2 Fugacity	0.2 atmospheres, fixed
CO_2 Fugacity	$10^{-3.4}$ atmospheres, fixed
Assumed [Si]	2.8 mg/L, ~equilibrium with quartz
Charge Balance	$SO_4^{=}$
Activity Model	Extended Debye-Huckel
Suppressed Minerals	
Hematite	$CuCr_2O_4$
Goethite	$NiFe_2O_4$
Pyrolusite	$Co(FeO_2)_2$
$Ba_3(AsO_4)_{2(c)}$	Co_3O_4
$CuFeO_{2(c)}$	Co_2SiO_4
$Cu_3(AsO_4)_{2(c)}$	Ferrite (Cu, Zn, Mg, Ca)

1004

1005

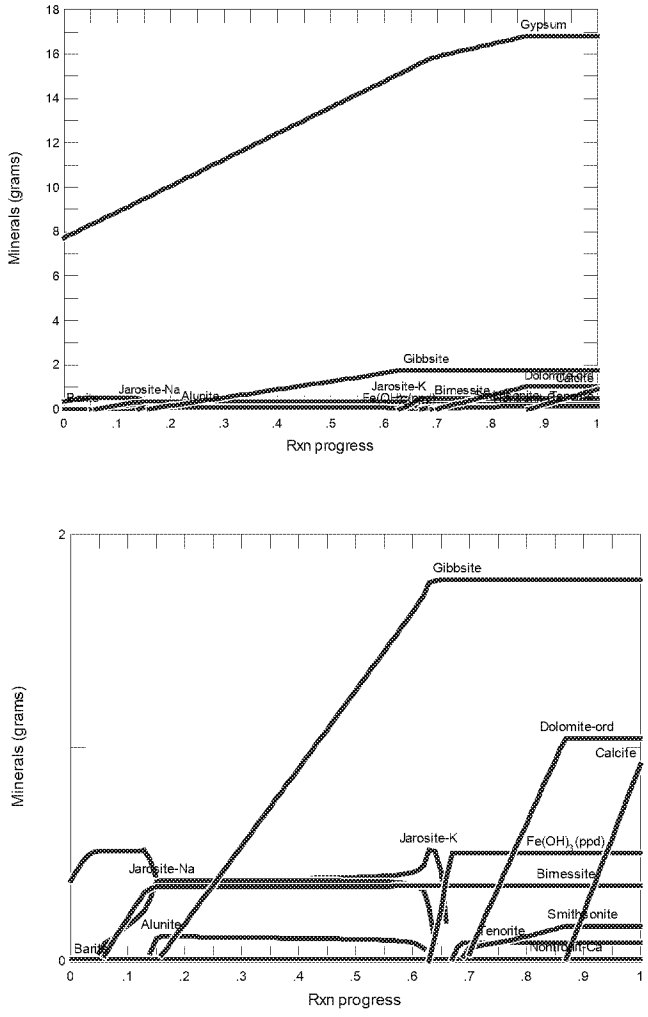

1006

1007 **Figure C-9. Simulation of the reaction of "Peak Concentration" release waters (Table 2) flowing from**
1008 **Cement Creek with Animas River alkalinity: 9A depicts gypsum to be supersaturated initially, consistent**
1009 **with the conservative assumption of disregarding solubility constraints to estimate release water**
1010 **composition; 9B expands the y axis to show detail of the less-massive phases and indicates that Na-**
1011 **jarosite and barite were supersaturated initially as well. To perform this simulation, a mass of calcite**
1012 **($CaCO_3$) is chosen such that one kilogram of Peak Concentration release water (Table 2) is just barely**
1013 **saturated with calcite at reaction's end, consistent with the chemistry of the Animas at ≥150 km**
1014 **downstream from Gold King (Figure 8). Shown here, at reaction's end gibbsite ($Al(OH)_3$), ferrihydrite**
1015 **($Fe(OH)_3$), birnessite (MnO_2), gypsum ($CaSO_4 \cdot 2H_2O$) and dolomite ($CaMg(CO_3)_2$) are expected to have**
1016 **precipitated from solution. The saturated state of the Animas River with gypsum likely was short-lived**
1017 **and, after the sulfate-rich release waters migrated downstream, any gypsum that precipitated would have**
1018 **redissolved. Similarly dolomite might have dissolved after [Mg^{2+}] decreased. For these temporary phases,**
1019 **it is likely that they would have entrained trace metals within the lattice as impurities and, as they**
1020 **dissolve, the trace metals would have entered solution. These trace metals then would be scavenged by**
1021 **the hydroxide minerals as they migrated down the Animas as described in the text.**

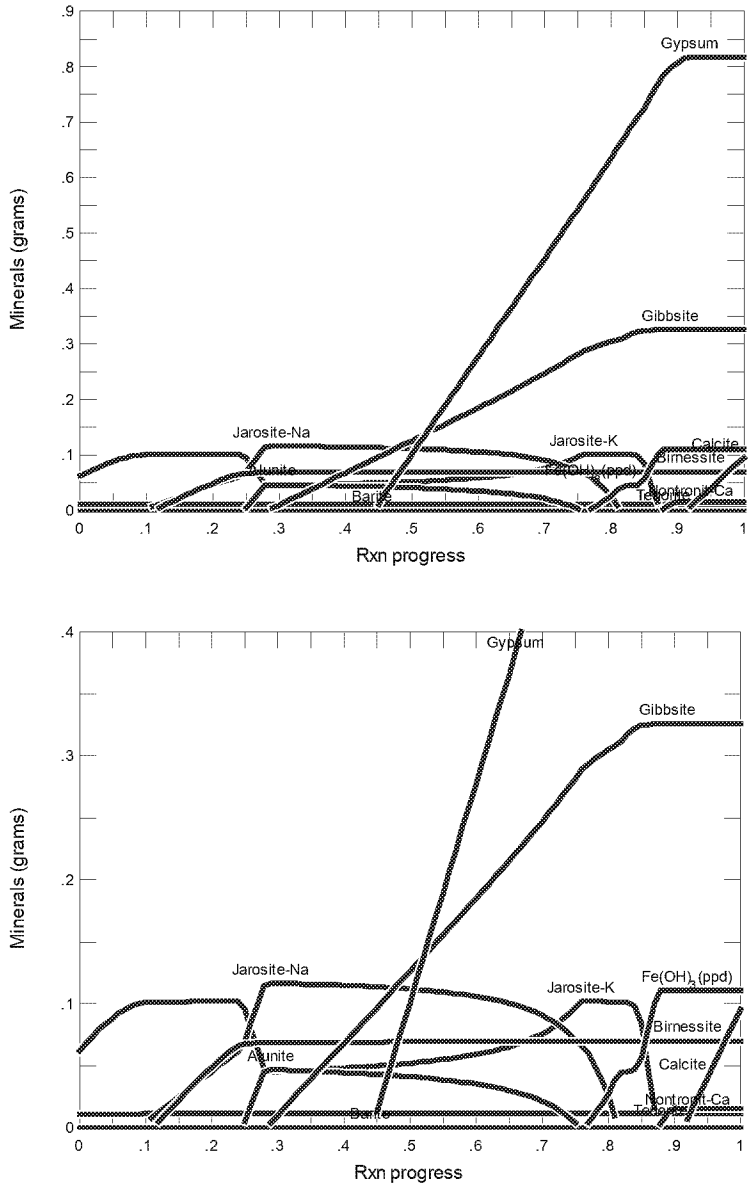

1022

1023 **Figure C-10. Simulation of reaction of Plume + Background Mean concentrations with Animas alkalinity.**
1024 **The masses of minerals precipitated from one kg of solution (plotted on the y axis), along with the**
1025 **calculated discharge of 11.42 ML, can be used to estimate masses of minerals precipitated from the**
1026 **waters released during plume discharge from Cement Creek (Figure 11).**

1027

1028

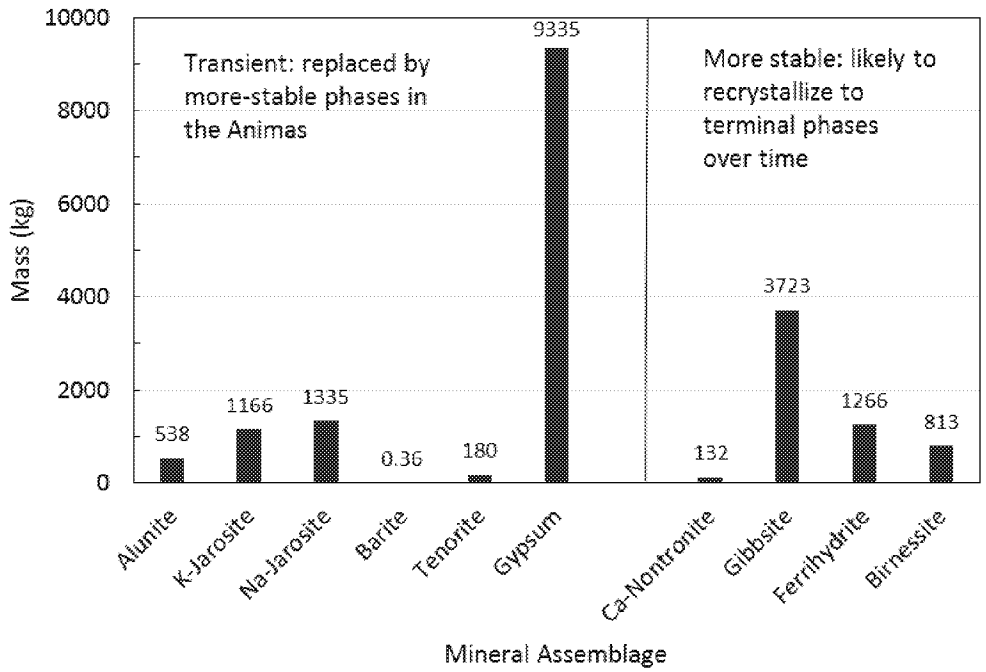

Figure C-11. Masses of minerals precipitated from the release waters (and Cement Creek water flowing with release waters) as these waters intermingled and reacted with Animas River water as estimated from thermodynamic modeling of titration of "Plume + Background Mean" water with calcite alkalinity that is present in the Animas (Figure 10). Cations initially in alunite and jarosite likely will ultimately enter the more stable gibbsite and ferrihydrite phases, respectively. Whether low trace levels of Ba and Cu will form discrete mineral phases such as barite and tenorite, respectively, or sorb to and isomorphically substitute directly in more-stable mineral phases is uncertain, but ultimately these ions likely will be bound to more stable minerals and their aqueous concentrations maintained at low levels as suggested by modeling described later in this report. Gypsum, likely will be unstable in the low-$SO_4^=$ waters of the Animas; comprised of Ca^{2+} and $SO_4^=$, these innocuous ions will migrate downstream. Nontronite ($Ca_{0.165}Fe_2Al_{0.33}Si_{3.67}O_{10}(OH)_2$) is a commonly occurring smectite clay mineral. Gibbsite, ferrihydrite and birnessite are commonly occurring oxyhydroxide minerals and likely will recrystallize to similar, but still more stable, phases over time, as elaborated upon later. The modeled masses of metals bound in the four "more stable" minerals are Fe = 700 kg, Al = 1290 kg, and Mn = 510 kg.

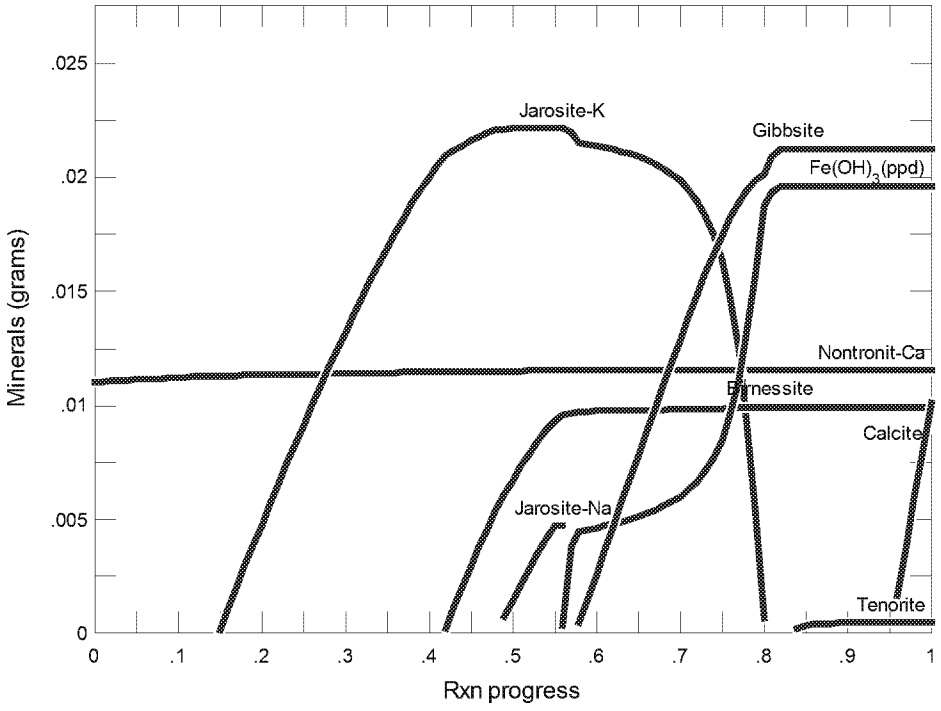

Figure C-12. Simulation of the reaction of Cement Creek Background Mean solutes with Animas alkalinity. It is noteworthy that this thermodynamic modeling suggests jarosite precipitates from solution for Cement Creek background waters alone. Like with the plume waters, however, jarosite is replaced by more stable hydroxide mineral phases.

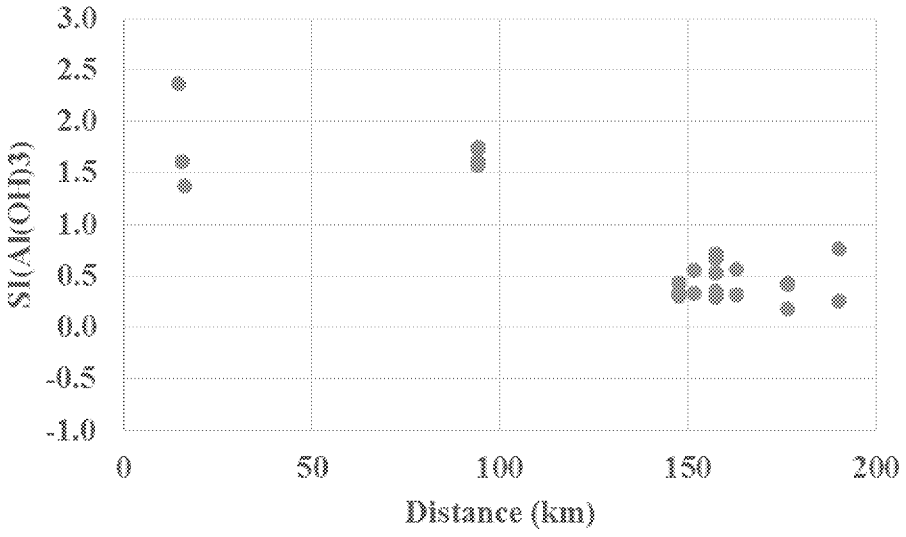

1051

1052 **Figure C-13. Saturation indices (SIs) with respect to gibbsite ($Al(OH)_3$) vs distance from Gold King Mine.**
1053 **The positive SI values suggest saturation with the mineral gibbsite limited the dissolved concentration of**
1054 **aluminum. Many additional samples were analyzed for aluminum (as reflected in the large number of**
1055 **sample points depicted in Figure 8), but aluminum fell below the reporting limit in these other samples.**
1056 **Few sulfate data are available for the southern Animas but, using the mean of the available $SO_4^=$ data and**
1057 **thermodynamic data from Geochemist's Workbench, the saturation index for alunite indicates gross**
1058 **undersaturation (SI alunite ~ -18).**

1059

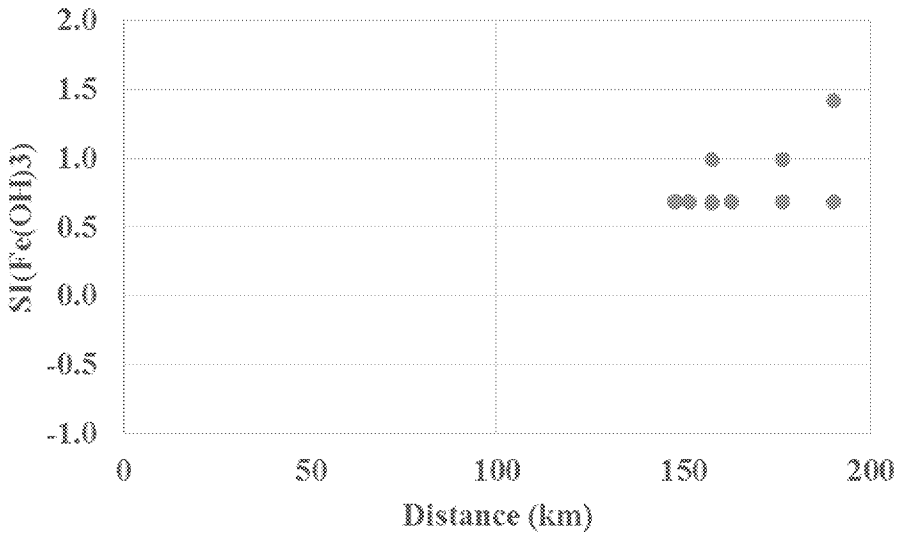

1060

1061 **Figure C-14. Saturation indices (SIs) with respect to ferrihydrite ($Fe(OH)_3$) vs distance from Gold King Mine.**
1062 **These data indicate saturation with respect to ferrihydrite. Many additional samples were analyzed for**
1063 **iron (as reflected in the large number of sample points depicted in Figure 8), but iron fell below the**
1064 **reporting limit in these other samples. Few sulfate data are available for the southern Animas but, using**
1065 **the mean of the available $SO_4^=$ data and thermodynamic data from Geochemist's Workbench, the**
1066 **saturation index for K-jarosite indicates gross undersaturation (SI alunite ~ -9).**

1067

1068 **Table C-5. Typical particle size, diagenetic times for selected Al and Fe oxides under surficial conditions**

Mineralization Phase	Size Range (1)	Size Reference	Formation Time Scale (6)	Time Reference	Zero Point of Charge	ZPC Reference
Aluminum Oxide						
amorphous $Al(OH)_3$ nucleation	<100 nm	2	≤24 hours	4	8.0 -9.2	11
amorphous $Al(OH)_3$ flocs/aggregates	2 µm - 2 mm	3 & 4	seconds to hours		8.0 -9.2	11
microcrystalline gibbsite aggregates	2 µm - 2 mm	3 & 4	2 to 20 weeks	4	8.0 -9.2	11
crystalline gibbsite aggregates	2 µm - 2 mm	3 & 4	~2 years	4	8.0 -9.2	11
kaolinitic clay aggregates	2 µm - 2 mm	3 & 4	years to millenia	7		
Ferric Oxide						
amorphous $Fe(OH)_3$ nucleation	2 - 7 nm	5	seconds to hours	8	7.9 - 8.2	12
2-line ferrihydrite flocs/aggregates	2 µm - 2 mm	3	seconds to hours		7.9 - 8.2	12
6-line ferrihydrite aggregates	2 µm - 2 mm	3	≥1 - 3 year	9	7.9 - 8.2	12
goethite or hematite aggregates	2 µm - 2 mm	3	≥1 - 3 year	9 & 10	9.0-9.7 or 8.5	13

1069

1070 1) Single grain for incipient nucleation, aggregates for later phases, as is their habit
1071 2) Hsu, 1989, p. 340
1072 3) Schwertmann & Taylor, 1989, p. 417; given common, extensive co-substitution of Al & Fe in oxides
1073 4) Nordstrom et al., 1984, p. 35
1074 5) Schwertmann & Taylor, 1989, p. 392; Cornell and Schwertmann, 2003, p. 78
1075 6) Formation time scale is under a variety of laboratory idealized surficial conditions. Actual times can
1076 vary drastically.
1077 7) Langmuir, 1997, p. 252
1078 8) Cornell & Schwertmann, 2003, p. 207
1079 9) Cornell & Schwertmann, 2003, p. 207; Kukkadapu, et al., 2003
1080 10) Cornell & Schwertmann, 2003, p. 207; Kukkadapu, et al., 2003; Schwertmann & Cornell, 2000, p.
1081 110
1082 11) Hsu, 1989
1083 12) Dzombak & Morel, 1990
1084 13) Sverjensky, 1994

1085

1086

1087 **Table C-6. Estimation of dissolved metal concentrations in equilibrium with $Fe(OH)_3$ solids at the pH of the**
1088 **Animas River and Comparison with Observed Values at Four River Locations**

Site		Durango	NAR	Aztec	Farmington
Distance from GKM (km)		95	132	163	190
Date/Time of Plume Peak		8/7/15 2:00 AM	8/7/15 2:30 PM	8/8/15 3:00 AM	8/8/15 10:45 AM
Peak Total Concentrations (mg/l)	Fe	226.27	76.40	33.76	17.36
	As	0.11	0.06	0.03	0.02
	Cu	0.47	0.23	0.12	0.08
	Pb	3.14	1.41	0.54	0.39
	Zn	1.18	0.54	0.42	0.31
Peak Dissolved Concentrations (mg/l)	Fe	2.2770	0.4500	0.0449	0.0199
	As	0.0008	0.0004	0.0006	0.0009
	Cu	0.0071	0.0023	0.0013	0.0019
	Pb	0.0004	0.0031	0.0002	0.0002
	Zn	0.1399	0.0110	0.0028	0.0033
	pH (SU)	7.42	8.00	7.90	8.11
Log K_e	As	-9.68	-10.40	-10.25	-10.58
	Cu	-3.34	-2.96	-3.04	-2.93
	Pb	-5.10	-4.72	-4.80	-4.69
	Zn	-1.44	-1.06	-1.14	-1.03
Modeled Dissolved Concentrations (mg/l)	As	0.1050	0.0577	0.0260	0.0193
	Cu	0.0071	0.0023	0.0013	0.0019
	Pb	0.0004	0.0031	0.0002	0.0002
	Zn	0.1400	0.0110	0.0028	0.0033
Modeled/Peak Dissolved Ratio	As	127.29	144.26	44.77	21.71
	Cu	1.00	1.00	1.00	1.00
	Pb	1.00	1.00	1.00	1.00
	Zn	1.00	1.00	1.00	1.00

1089

1090

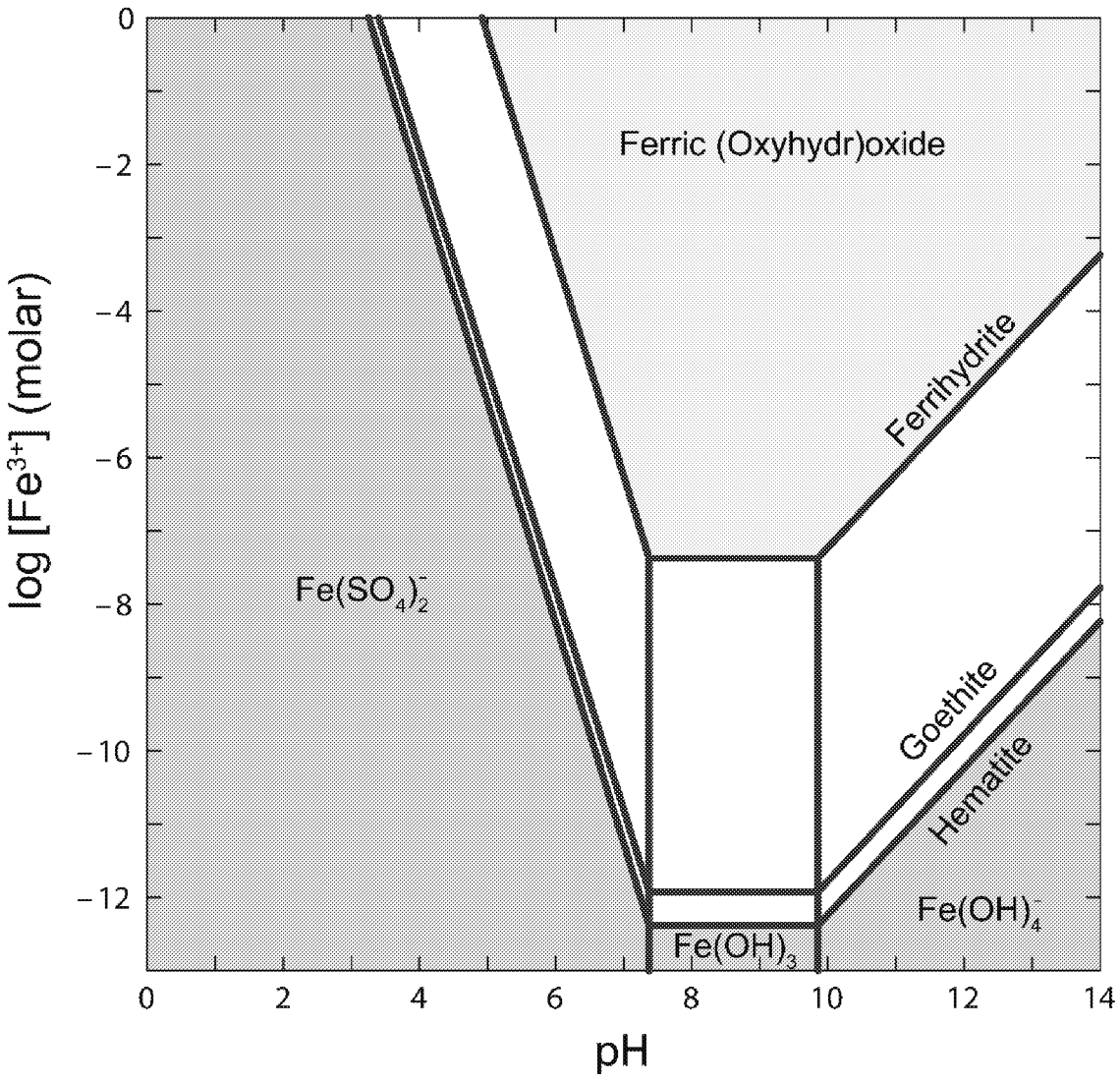

Figure C-15. Stability fields of ferric oxide minerals as a function of $[Fe^{3+}]$ and pH, with $[SO_4^{=}]$ = 90 mg/l, similar to conditions expected in the upper Animas. Generally, as waters become supersaturated with mineral phases, say by an increase in pH, less thermodynamically stable mineral phases will precipitate first, e.g., amorphous $Fe(OH)_3$ or stoichiometric ferrihydrite. Over time these incipient mineral phases recrystallize to more stable forms, e.g., goethite or hematite as shown here. As these minerals recrystallize to more stable forms, they equilibrate with progressively lower solution activities. Thermodynamic data as reported in Geochemist's Workbench (Bethke 1998).

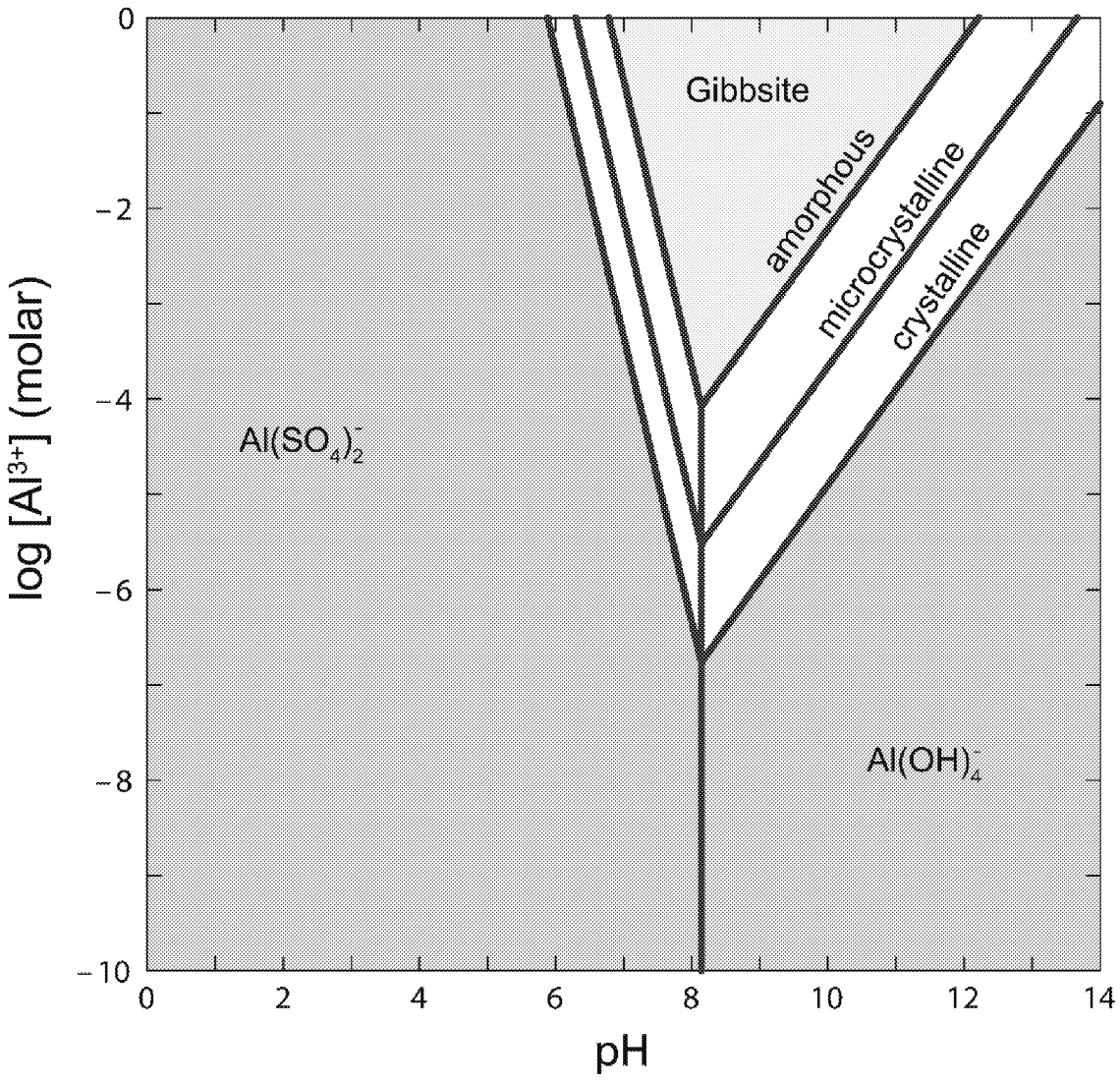

Figure C-16. Stability fields of aluminum oxide minerals as a function of $[Al^{3+}]$ and pH, with $[SO_4^{=}]$ = 90 mg/l, similar to conditions expected in the upper Animas. Generally, as waters become supersaturated with mineral phases, say by an increase in pH, less thermodynamically stable mineral phases will precipitate first, e.g., amorphous $Al(OH)_3$. Over time these incipient mineral phases recrystallize to more stable forms, e.g., microcrystalline and crystalline gibbsite. As these minerals recrystallize to more stable forms, they equilibrate with progressively lower solution activities. Thermodynamic data for Al as reported in Nordstrom et al. (Nordstrom et al. 1984) with additional data from Geochemist's Workbench (Bethke 1998).